Materials Today Bio 30 (2025) 101372

Contents lists available at ScienceDirect

Materials Today Bio

journal homepage: www.journals.elsevier.com/materials-today-bio

High paracrine activity of hADSCs cartilage microtissues inhibits extracellular matrix degradation and promotes cartilage regeneration

Wei Liu [a,b,1], Hongyu Jiang [a,d,1], Jiajie Chen [a,e,1], Yue Tian [c,1], Ying He [a], Ying Jiao [b], Yanjun Guan [a], Zhibo Jia [a], Yanbin Wu [a], Cheng Huang [a,d], Yiben Ouyang [a,e], Wenjing Xu [a], Jianhong Qi [b,***], Jiang Peng [a,e,**], Aiyuan Wang [a,e,*]

[a] Institute of Orthopedics, The Fourth Medical Center of Chinese PLA General Hospital, Beijing Key Lab of Regenerative Medicine in Orthopedics, Key Laboratory of Musculoskeletal Trauma & War Injuries PLA, No. 51 Fucheng Road, Beijing, 100048, PR China
[b] College of Sports Medicine and Rehabilitation, Shandong First Medical University & Shandong Academy of Medical Sciences, Taian, Shandong, 271016, PR China
[c] The Second Medical Center of Chinese PLA General Hospital, PR China
[d] Department of Orthopedic, The Affiliated Hospital, Southwest Medical University, Luzhou, PR China
[e] School of Medicine, Nankai University, Tianjin, 300071, PR China

ARTICLE INFO

Keywords:
Cartilage regeneration
Microtissues
Mesenchymal stem cells
Paracrine secretion
ECM degradation

ABSTRACT

Due to its unique structure, articular cartilage has limited self-repair capacity. Microtissues are tiny tissue clusters that can mimic the function of target organs or tissues. Using cells alone for microtissue construction often results in the formation of necrotic cores. However, the extracellular matrix (ECM) of native cartilage can provide structural support and is an ideal source of microcarriers. Autologous adipose-derived mesenchymal stem cells (ADSCs) and bone marrow mesenchymal stem cells (BMSCs) are widely used in cartilage tissue engineering. In this study, we fabricated microcarriers and compared the behavior of two homologous cell types in the microcarrier environment. The microcarrier environment highlighted the advantages of ADSCs and promoted the proliferation and migration of these cells. Then, ADSCs microtissues (ADSCs-MT) and BMSCs microtissues (BMSCs-MT) were fabricated using a three-dimensional dynamic culture system. In vitro and *in vivo* experiments verified that the cartilage regeneration ability of ADSCs-MT was significantly superior to that of BMSCs-MT. Transcriptomics revealed that ADSCs-MT showed significantly lower expression levels of ECM degradation, osteogenesis, and fibrocartilage markers. Finally, the protective effect of microtissues on inflammatory chondrocytes was validated. Overall, the ADSCs-MT constructed in this study achieved excellent cartilage regeneration and could be promising for the autologous application of cartilage microtissues.

1. Introduction

The extracellular matrix (ECM) is the most abundant component of cartilage tissue, accounting for about 90 % of its volume [1]. ECM is primarily composed of macromolecules such as glycoproteins, collagens, and proteoglycans, which are crucial for the maintenance of tissue morphology, differentiation, and homeostasis. The orderly arrangement of the ECM confers cartilage with unique mechanical and biochemical characteristics [2], playing a key role in the response to mechanical stimuli at joints and providing cushioning and lubrication. Furthermore, the ECM offers a stable microenvironment for chondrocytes and regulates various cellular processes, including proliferation, migration, differentiation, and metabolism [3].

Articular cartilage has a limited ability to repair itself [4].

* Corresponding author. Institute of Orthopedics, The Fourth Medical Center of Chinese PLA General Hospital, Beijing Key Lab of Regenerative Medicine in Orthopedics, Key Laboratory of Musculoskeletal Trauma & War Injuries PLA, No. 51 Fucheng Road, Beijing, 100048, PR China.
** Corresponding author. Institute of Orthopedics, The Fourth Medical Center of Chinese PLA General Hospital, Beijing Key Lab of Regenerative Medicine in Orthopedics, Key Laboratory of Musculoskeletal Trauma & War Injuries PLA, No. 51 Fucheng Road, Beijing, 100048, PR China.
*** Corresponding author. College of Sports Medicine and Rehabilitation, Shandong First Medical University & Shandong Academy of Medical Sciences, Taian, Shandong, 271016, PR China.
E-mail addresses: jhqi7281@163.com (J. Qi), pengjiang301@126.com (J. Peng), aiyuanwang301@126.com (A. Wang).
[1] Wei Liu, Hongyu Jiang, Jiajie Chen and Yue Tian contributed equally to this work.

https://doi.org/10.1016/j.mtbio.2024.101372
Received 4 September 2024; Received in revised form 21 November 2024; Accepted 25 November 2024
Available online 29 November 2024

Irrespective of whether the injury is traumatic or disease-induced, cartilage tissues induce inflammatory changes, such as the release of inflammatory mediators like tumor necrosis factor (TNF-α), interleukin 1β (IL-1β), and chemokines [5,6]. Additionally, they promote an increase in matrix-degrading enzymes, such as matrix metalloproteinases (MMPs) and ADAMTS family [7], which not only destroy the structure of the ECM but also produce degradation products that trigger stronger inflammatory responses and promote the gradual degradation of the ECM through the loss of collagen and proteoglycan components [8]. This affects a series of cellular and stromal functions and causes subchondral bone damage, resulting in osteophyte formation. Joints also suffer other detrimental effects, such as the destruction of biomechanical features, pain, loss of function, and restricted movement [9]. Currently, the clinical treatments for articular cartilage injuries primarily include medication (e.g., injection of hyaluronic acid and steroids into the joint cavity), physical therapy (e.g., physical rehabilitation training), and surgery (e.g., microfracture surgery and arthroplasty) [10,11]. Although these interventions can alleviate symptoms and promote cartilage repair to varying degrees, they are associated with limitations such as accelerated joint degeneration, high surgical trauma, and insufficient regeneration, which make it challenging to achieve structural and functional ECM repair [12]. However, biomaterials are often used in the field of regenerative medicine for assembly and repair, with cartilage-derived decellularized ECM (cECM) serving as one of the more mature biomaterials for this purpose [13].

ECM decellularization enables the removal of cellular components and other antigenic elements, which reduces the risk of inflammatory reactions and immune rejection while preserving the biological, mechanical, and biochemical characteristics of the ECM [4,8,9]. Hence, decellularized ECM can serve as a reliable three-dimensional (3D) carrier for subsequent cell seeding [13]. Poly lactic-co-glycolic acid (PLGA) is a common synthetic polymer used in biomaterials, but it tends to induce inflammation. To address this issue, Kim S et al. combined cECM with PLGA and found that the addition of cECM inhibits inflammatory cytokines and reactive oxygen species, enhances cell proliferation, and promotes chondrogenic differentiation [14]. Additionally, Jeanne E et al. found no significant difference in the content of transforming growth factor β1(TGF-β1) — an important matrix-bound growth factor that supports cell proliferation and is crucial for articular cartilage — between natural and decellularized cartilage [15].

Tissue engineering often achieves the re-proliferation of scaffolds through recellularization, thereby requiring constructs with specific structures and functions [16]. Stem cells are widely used for recellularization due to their strong proliferation and differentiation capabilities. Among such stem cells, embryonic stem cells (ESCs) and induced pluripotent stem cells (iPSCs) exhibit the greatest growth and differentiation potential. However, their use is associated with ethical concerns, and their differentiation into specific cell lineages is quite time-consuming [17,18]. In contrast, mesenchymal stem cells (MSCs) are widely utilized in cartilage tissue engineering owing to their excellent immune properties and chondrogenic differentiation abilities [19–21]. Additionally, compared to chondrocytes, MSCs can be autologously obtained through less invasive procedures [22]. Although allogeneic MSCs theoretically reduce the risk of immune rejection, studies have shown that they have significantly lower survival rates than autologous MSCs and can promote the production of T cells with memory phenotypes [21,23].

In regenerative medicine, traditional scaffold implantation often requires large surgical incisions and carries the risk of complications such as pain and infection. However, the minimally invasive implantation of microtissues can prevent these issues and enable the flexible repair of irregularly shaped cartilage defects [24,25]. Microtissues are usually referred to as the aggregation of seed cells in the action of a cell-to-cell or cell-to-extracellular matrix by a variety of means forming microscopic tissues with diameters between 100 and 1000 μm [26–28]. In the field of cartilage tissue engineering, microtissues have been shown to be useful for generating relatively homogeneous ECM cartilage-like tissues, which can also be used as building blocks for repairing cartilage defects [25,29]. Unlike organoids, which are composed of multiple organ-specific cell types and require precise and stringent control of cytokines and culture conditions [30], microtissues are relatively less stringent in terms of construction, culture conditions, and cost. Micromass and pellet cultures are classically used in cartilage microtissue therapy and research [31]. However, these microtissue cores often exhibit issues such as necrosis, incomplete differentiation, and the up-regulation of COL1 and COL10 during culture [32]. Nevertheless, the use of cECM to construct microtissues can help in addressing these issues effectively. Previous studies have shown that cECM-based microtissues promote rapid cell proliferation and chondrogenesis [33]. Additionally, the distinct physical and chemical characteristics of cECM and its 3D structure support the proliferation and differentiation of resident cells, such as MSCs and chondrocytes [4].

In this study, we utilized two prominent sources of autologous MSCs — adipose-derived stem cells (ADSCs) and bone marrow-derived stem cells (BMSCs) — to construct and systematically compare microtissues. Both ADSCs and BMSCs are readily available through ethical means, and their application prospects have been thoroughly validated. BMSCs were the first MSCs used in tissue engineering and can differentiate into a wide range of tissues [34]. However, ADSCs, which are easier and more readily available from subcutaneous fat, have also shown notable regenerative advantages in cartilage repair, causing less damage. Notably, the regenerative potential of ADSCs and BMSCs can vary depending on the scaffold and treatment environment. For instance, in Xie et al.'s study, BMSCs inoculated into PRP scaffolds were found to demonstrate higher proliferation rates and produce greater amounts of cartilage-specific matrix than ADSCs [22]. Conversely, Wang et al. reported that hypoxic treatments can enhance the differentiation potential of ADSCs, effectively alleviating cartilage damage in animal models [35].

While numerous studies have explored the chondrogenic capacity of these two types of cells [36], systematic evaluations and comparisons of these cells in the context of microtissue construction are quite limited. Therefore, it is crucial to compare the performance of ADSCs and BMSCs in microtissues to advance their clinical application. Moreover, Sulaiman et al. have demonstrated that MSCs in gelatin microspheres show better proliferation and cartilage formation abilities in dynamic cultures than under static conditions [19]. Similarly, MSC microtissue polymers have been found to demonstrate faster ECM generation rates under the dynamic culture conditions provided by a rotating bioreactor [37]. Thus, in this study, we employed a three-dimensional dynamic culture strategy to cultivate and expand microtissues in a nutrient-rich, mechanical environment prior to transplantation, which helped mitigate the risks associated with necrotic cores and physical detachment.

Our study aimed to explore the chondrogenic capacity and regenerative effects of microtissues derived using ADSCs and BMSCs (ADSCs-MT and BMSCs-MT) under both *in vitro* and *in vivo* conditions. Initially, we performed comparative functional studies on ADSCs and BMSCs obtained from homologous sources to understand the initial state and function of the two groups of cells. Then, *in vitro* studies were performed to compare the structures and properties of ADSCs-MT and BMSCs-MT and evaluate their effects on inflammatory chondrocytes within an inflammatory environment. Additionally, we performed mRNA sequencing on both types of microtissues to compare their molecular performance. Finally, we assessed the *in vivo* effects of ectopic chondrogenesis induced by the microtissues by subcutaneously implanting ADSCs-MT and BMSCs-MT in nude mice. An overview of the study design is provided in Fig. 1. The results indicated that autologous ADSCs-MT demonstrate better cellular activity and chondrogenic properties, exhibiting enhanced paracrine effects and providing a stronger inhibition of ECM degradation than BMSCs-MT.

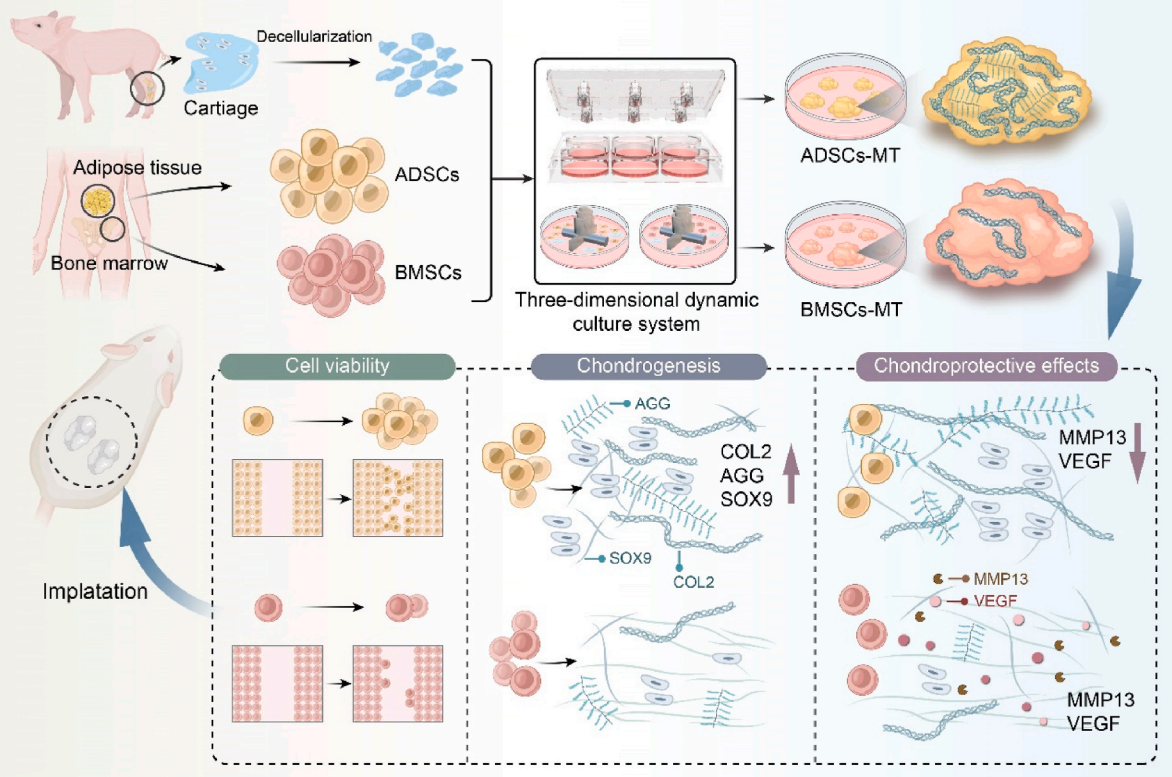

Fig. 1. Schematic diagram showing the preparation of ADSCs microtissues and BMSCs microtissues using cECM microcarriers, and *in vivo* and *in vitro* validation of cartilage regeneration through the use of ADSCs cartilage microtissues.

2. Methods

2.1. Preparation and characterization of cECM microcarriers

2.1.1. Preparation of cECM microcarriers

The hindlimb knee joint cavity was opened under aseptic conditions to obtain hyaline cartilage slices at the trochlea femoris. The tissue was shock-treated in 10mM Tris-HCl (Sigma, USA) at 37 °C for 12 h and in 1 % SDS (Sigma, USA) at 37 °C for 48 h. After each treatment step, the tissues were washed and shaken thrice in PBS (Gibco, USA) for 10 min each time. Finally, the tissues was cleaned and shaken thrice in PBS, 2 h each time. The decellularized cartilage slices were crushed using a tissue grinder (QIAGEN, Germany), and the powder was sieved to obtain microcarriers with a diameter of 150–300 μm. The microcarriers were subsequently sterilized using ^{60} Coγ and stored at 4 °C.The cECM microcarriers were imaged using a bright-field microscope (Nikon, Japan), and their particle size was analyzed using ImageJ software.

2.1.2. Detection of residual DNA, collagen, and glycosaminoglycan (GAG)

Untreated and decellularized samples were freeze-dried for 24 h, weighed, and placed in a DNA extraction analyzer (QIAGEN, Germany) for total DNA extraction. The extracted DNA was quantified using a DNA quantitative test kit (Invitrogen, USA) according to the manufacturer's instructions. The test samples and standards were examined for fluorescence intensity using an Infinite 200 Pro system (TECAN, China) at an excitation wavelength of 480 nm and emission wavelength of 520 nm. A standard curve was drawn, and the DNA content of cartilage before and after decellularization was measured. For the detection of matrix components, the samples were used for the quantitative detection of hydroxyproline and GAG before and after decellularization using the hydroxyproline assay kit (Jiancheng, China) and the DMMB colorimetric kit for total tissue GAG content (GenMed, Germany), respectively, based on the manufacturer's instructions. Hydroxyproline accounted for 13.4 % of total collagen.

2.1.3. Histological and DAPI staining

Untreated and decellularized cartilage slices were fixed in tissue fixative (Solarbio, China) for 30 min and then cut into 10-μm-thick sections using a cryosectioning machine (Leica, Germany). Tissue morphology and structure were assessed using hematoxylin and eosin (H&E) staining (Solarbio, China), and the proteoglycans in the matrix were visualized using Alcian Blue and Safranin O staining (Solarbio, China). Cell nuclei were visualized using DAPI staining (Solarbio, China).

2.1.4. Scanning electron microscopy (SEM)

The microcarriers were first fixed in 2.5 % glutaraldehyde (Solarbio, China) for 24 h and then rinsed thrice in PBS. The samples were dehydrated using a gradient of ethanol concentrations. This was followed by critical point drying and the vacuum sputtering of platinum ions. Finally, SEM (Thermo Fisher Scientific, USA) was used to observe and image the microcarriers.

2.2. Extraction, cultivation, identification, and cell behavior evaluation of hADSCs and hBMSCs

2.2.1. Extraction and cultivation of hADSCs and hBMSCs

The isolation and culture of hADSCs and hBMSCs were approved by the Ethics Committee of the Fourth Medical Centre of the General Hospital of the People's Liberation Army (2020KY036-HS001). These cells were obtained from the subcutaneous adipose tissue and bone marrow of patients undergoing hip joint repair surgery. The adipose tissue was treated with an equal volume of 0.1 % type I collagenase (Sigma, USA) for 40 min at 37 °C in an incubator. Then, Dulbecco's Modified Eagle Medium/F12 (DMEM/F12, Novozymes Biologics, China) containing 10 % fetal bovine serum (FBS, Novozymes Biologics, China) was added to terminate collagenase digestion. The adipose layer and supernatant were removed via centrifugation, and the cells were washed with 10 mL of PBS (Gibco, USA) and re-centrifuged. The cells

were resuspended in DMEM/F12 containing 10 % FBS in a 75 cm^2 culture bottle (Corning, USA) for cultivation. Meanwhile, bone marrow was treated as described by C Xie et al. to obtain hBMSCs [38]. The cells were separated by filtration through a 40-μm cell filter (Corning, USA) and centrifuged and resuspended in 75 cm^2 culture flasks.

Both groups of cells were cultured at 37 °C in an incubator containing 5 % CO_2 for 3–4 d. Then, the medium was replaced with mesenchymal stem cell medium (MSCM, ScienCell, USA), and the culture was continued by adding fresh medium every 3 d. When the cell fusion rate reached about 90 %, the cells were digested with TrypLE Express (Gibco, USA) for passaging. Cells from generations 3–7 were used in the present cells.

2.2.2. Identification of hADSCs and hBMSCs

Morphological observation: The morphological observation and imaging of the 3rd-generation hADSCs and hBMSCs were performed under a light microscope (Nikon, Japan).

Flow cytometry analysis: The digested cells were stained using antibodies (BioLegend, USA) against CD90, CD105, and CD73 and negatively labeled with CD34 and CD45. Unstained cells were used as negative controls, and the two groups of cells were detected using flow cytometry (BD, USA).

Induction of differentiation: The two groups of cells were cultured for 14 days before treatment with an induction solution for osteogenic and adipose tissue differentiation (Fuyuanbio, China). Then, the osteogenic ability of the cells was evaluated using Alizarin red staining, and the adipogenic ability was evaluated using oil red O staining. Chondrogenic differentiation experiments were performed using microsphere aggregation cultures. Both groups of cells were cultured for 21 days in an induction solution that promoted differentiation to cartilage tissue (Cyagen, China). The microspheres were cryosectioned, fixed, and then stained with Alcian Blue before observation and imaging under a microscope.

2.2.3. Effects of the cECM environment on cell proliferation

The cECM extraction solution was obtained by soaking the ^{60}Co-sterilized microcarriers in complete MSCM containing 5 % FBS at a mass concentration of 0.2 g/mL for 72 h at 37 °C.

Ki67 fluorescence staining: The two groups of cells were inoculated in 24-well plates (1×10^4 cells per well, with coverslips) and incubated in cECM extract for 24 h. In the control groups, the two types of cells were incubated in MSCM containing 5 % FBS. Then, the cells were fixed with a fixative for 12 min, treated with 0.5 % Triton (Solarbio, China) for 9 min to permeabilize the cell membrane, and blocked with 10 % goat serum (Solarbio, China) for 2 h. Subsequently, the cells were incubated overnight with an anti-Ki67 primary antibody (1:200, Abcam, UK) at 4 °C. On the second day, the cells were incubated with a fluorescently conjugated secondary antibody (1:200, Abcam, UK) for 1 h before three washes with PBS. Then, the cells were treated with 4,6-dimercapo2-phenylindle (DAPI, Solarbio, China) for 5 min. Finally, the cells were imaged under a fluorescence microscope (Nikon, Japan).

CCK-8: The two groups of cells were inoculated in 96-well plates (3×10^3 cells per well) and incubated in the cECM extract. Cells cultured in complete medium only were used as the control. The Cell Counting Kit-8 (CCK-8, Beyotime, China) assay was used to evaluate the proliferation of the cells. After treatment, the CCK-8 reagent was added to the well on days 1, 3, and 5. The cells were incubated for 2 h, and their absorbance was measured after removing the supernatant from each well.

2.2.4. Effect of cECM environment on the migration of two types of cells

Cell migration assay: The two groups of cells were inoculated in six-well plates (1×10^5 cells per well) and grown in complete medium until they covered 80–90 % of the well plate area. The cell monolayer was scratched with a 100-μL pipette tip perpendicular to a horizontal line marker, and the cells were then washed gently with PBS thrice. The cells were incubated in cECM extract, and cells cultured in complete medium were used as controls. Finally, the cells were observed and imaged under a light microscope at 0 h and 24 h.

Transwell assay: Transwell chambers with a pore size of 8 μm (Corning, USA) were added to 24-well plates. The two types of cells (1×10^4 cells per well) were first seeded in the upper chamber of the Transwell insert and incubated with serum-free MSCM. Meanwhile, the cECM extract was added to the lower chamber. Cells incubated with complete medium in the lower chamber were used as controls. After 24 h of incubation at 37 °C under 5 % CO_2, migrating cells were stained with crystal violet (Solarbio, China) and counted.

2.3. Construction and evaluation of hADSCs and hBMSCs microtissues

2.3.1. Construction and characterization

Microtissues were prepared by loading the two groups of cells into cECM microcarriers. The cells were trypsinized, counted, and seeded in low-adhesion 6-well plates (4×10^5 cells/well), and microcarriers were added at a concentration of 2×10^4 cells/mg, i.e. 20 mg of microcarrier per well. The microtissues were cultured in a bio-rotation reactor (CytoNiche Biotech, China), as follows: (i) dynamic culture for 3 d (proliferation phase) in complete medium at 37 °C and 5 % CO_2, followed by (ii) dynamic culture for 14 d (differentiation phase) in chondrogenic induction medium, with half the medium being replaced with fresh medium every alternate day. The operation of the bioreactor included the loading cell stage and the expansion and differentiation stage. The loading cell stage was operated at 20 rpm for 1 min and 0 rpm for 30 min (one cycle), for a total of 48 cycles, and the expansion and differentiation stage was operated at 40 rpm [39].

The two types of microtissues were observed and imaged at five time points, namely, −3 d, −2.5 d, −2 d, 0 d, and 14 d. Here, 0 d marked the end of the proliferation stage. Then, micro-morphological observations of the two types of microtissue cultures were carried out at 0 d and 14 d using SEM.

2.3.2. Evaluation of chondrogenic differentiation ability

Quantitative real-time PCR (qRT-PCR): To evaluate the expression of chondrogenic genes in the two types of microtissues, the microtissues were subjected to qRT-PCR for chondrogenic markers (*ACAN*, *SOX9*, and *COL2*). The primer sequences are shown in Table S1. Total RNA was extracted from the two types of microtissues cultured for 0 d and 14 d using the Total Cellular RNA Isolation Kit (QIAGEN, Germany). Then, the total mRNA was reverse-transcribed into cDNA using the PrimeScript RT kit (TOYOBO, Japan). Finally, qRT-PCR was performed using SYBR PreMix EX TAQ (Genstar, China) for amplification. The mRNA levels of all tested genes were normalized to those of *GAPDH*, and the relative gene expressions were calculated based on the $2^{-\Delta\Delta CT}$ method.

Western blot analysis: Microtissues were lysed with RIPA buffer (Solarbio, China) containing protease and phosphatase inhibitors. Proteins from microtissue lysates were then separated using 10 % SDS-PAGE (Beyotime, China) and transferred to PVDF membranes (Beyotime, China). The membranes were sealed in 5 % BSA sealing solution (Solarbio, China) for 1 h and then incubated with anti-ACAN (1:500, Abcam, UK) and anti-COL2 (1:500, Abcam, UK) antibodies at 4 °C overnight. The membranes were then washed and incubated with an HRP-conjugated secondary antibody (1:200, Abcam, UK) for 1 h at room temperature. The bands were developed (Solarbio, China) and imaged (Syngene, UK).

Histological staining: The two groups of microtissues were fixed and cryosectioned into 10-μm sections. SOX9 (1:500, Abcam, UK) expression was examined using immunofluorescence analysis. Microtissue morphology and structure were evaluated using H&E staining, and the content of glycosaminoglycans was examined using Toluidine blue staining (Solarbio, China).

2.3.3. Analysis of chondrocyte recruitment ability

First, 1×10^4 human chondrocytes (Procell, China) were seeded into

the upper chambers of Transwell chambers (8 μm pore size) placed in 24-well plates and cultured in DMEM/F12 serum-free medium. The lower chambers were filled with DMEM/F12 + 10 % FBS, DMEM/F12+hADSCs-MT, or DMEM/F12+hADSCs-MT. For groups involving the use of microtissues, set up 10 mg of microtissue per well. The cells were cultured at 37 °C under 5 % CO_2 for 24 h, and migrating chondrocytes were fixed, stained with 0.1 % crystal violet, and observed and imaged under a microscope.

2.4. RNA sequencing analysis

Three biological replicate samples of microtissues were prepared per group. After lysis with TRIzol (Solarbio, China) for 10 min, the samples were snap frozen in liquid nitrogen. The samples were then stored in a refrigerator at −80 °C and transported to Novogene Ltd. (China) on dry ice. Subsequent sample detection, library construction, and bioinformatic analysis were entrusted to Novogene Ltd. (China). After RNA extraction, an Agilent 2100 Bioanalyzer was used to accurately detect the integrity and total amount of RNA. Then, library construction and quality control were conducted. Samples that met quality control criteria were sequenced on an Illumina sequencing platform. Differential expression analyses between two groups were performed using DESeq2 software, with $p_{adj} \leq 0.05$ and $|\log2foldchange| \geqq 1$ used as the thresholds for significant differential expression. The differentially expressed genes (DEGs) were subjected to Gene Ontology (GO) enrichment analysis and Kyoto Encyclopedia of Genes and Genomes (KEGG) pathway analysis using clusterProfiler software.

2.5. Co-culture of chondrocytes and microtissues in an inflammatory environment

Chondrocytes and microtissues were co-cultured in an inflammatory environment using the Transwell system, as reported by Bin W et al. [40]. Chondrocytes (1×10^4 cells per well) were grown in a monolayer in the lower chamber of the Transwell insert, and three groups were established: DMEM/F12 + 10 % FBS, DMEM/F12 + hADSCs-MT, and DMEM/F12 + hBMSCs-MT. Groups involving microtissues were set up with 10 mg of microtissues per well and grown in the upper chamber of the Transwell system under liquid covered conditions. Before addition to the Transwell system, the chondrocytes were stimulated with IL-1β (10 ng/mL, MCE, China) for 48 h. Then, co-culture was performed at 37 °C under 5 % CO_2 for 7 d. Chondrocytes not subjected to inflammatory factor treatment were used as positive control. Chondrocytes were analyzed using qRT-PCR, western blot, and immunofluorescence assays to examine the expression of genes and proteins related to cartilage formation and degradation. The primer sequences are shown in Table. S1.

2.6. In vivo implantation of microtissues and evaluation of regenerated tissues

Eight-week-old immunodeficient male mice (BALB/c Nude) were randomly divided into three groups: GelMA group, GelMA + ADSCs-MT group, and GelMA + BMSCs-MT group (six mice in each group). Microtissue implants were prepared by adding 10 % (w/v) GelMA solution (EFL, China) and microtissues (5:1 vol ratio) to a mold (5 mm diameter and 2 mm height) and then irradiating them with blue light for 30 s to achieve a gelatinous structure. The implants for the GelMA group only contained 10 % (w/v) GelMA solution and were placed in PBS to keep them aseptically moistened. All mice were anesthetized with 1 % sodium pentobarbital. A 1-cm-long skin incision was made on the backs of the mice, and two subcutaneous pockets were created via blunt dissection. Implants from different groups were carefully implanted into the pockets, and the incisions were finally closed with 6-0 sutures (Ethicon, USA). The mice were sacrificed after 8 weeks, and the implants were collected and fixed overnight in 4 % paraformaldehyde before sectioning and evaluation with H&E staining, Safranin O staining, Toluidine blue, immunofluorescence assays, and immunohistochemistry.

Eight-week-old Sprague–Dawley male rats were randomly divided into five groups: the Control group (blank defect), the GelMA group, the ADSCs-MT group, the BMSCs-MT group, and the Sham group. Each group contained 6 rats. After the rats were anesthetized via the intramuscular injection of 3 % sodium pentobarbital, an incision was made on the medial side of the patella, and the patella was dislocated. Subsequently, the articular cartilage was exposed through the flexion of the knee joint. In the Sham group, after the dislocation of the patella, the patella was reset, and the joint capsule, muscle, and skin were sutured. In the other four groups, a ring drill with a diameter of 2 mm was used to create a 1.5-mm-deep defect in the groove of the pulley. Then, 10 % GelMA solution was directly injected into the defect in the GelMA group, while 10 % GelMA solution was injected to fill the gap and the surface of the defect in the ADSCs-MT and BMSCs-MT groups, respectively, and the defect was sealed following 30 s of blue light irradiation. The defects in the Control group were left untreated. Finally, the joint capsule, muscle, and skin were sutured in all four groups. Twelve weeks later, the rats were sacrificed, and the tissue was examined through gross visualization, Micro-CT analysis, and staining and quantitative scoring (Tables S2 and 3). The implants were collected, fixed in 4 % paraformaldehyde overnight, and then sectioned for histological evaluation. All the above procedures followed the National Institutes of Health (NIH) Guide for the Care and Use of Laboratory Animals and were approved by the Institutional Animal Care and Use Committee of Zhongyan Zichuang (Beijing) Biotechnology Co., LTD. (No. ZYZC202404019S).

2.7. Statistical analysis

GraphPad Prism 8.3 was utilized for statistical analysis. All experiments were performed using at least three independent samples, and all data were presented as the mean ± standard deviation (SD). The student's t-test was used when comparing two groups of data, one-way analysis of variance (ANOVA) was used to compare the means of multiple groups, and SNK-q was used to compare pairs across multiple groups. $p < 0.05$ was considered statistically significant.

3. Results

3.1. Preparation and characterization of cECM microcarriers

Histological and DAPI staining showed that after decellularization, the cellular structure of the cartilage (mainly in the nucleus) was disrupted (Fig. 2A), but most of the ECM was retained(Fig. 2A–E-F). DNA quantification provided a clearer picture of decellularization efficiency, demonstrating that the DNA content was significantly reduced after decellularization (0.0040 ± 0.0028 vs 0.4822 ± 0.222 μg/mg) (Fig. 2D). Light microscopy showed that after physical crushing and sieving, cECM microcarriers sized between 150 and 300 μm were obtained (Fig. 2B). Particle size analysis showed that the diameter of the microcarriers was 241.70 ± 46.98 μm(Fig. 2G). Further SEM analysis showed that the cECM microcarriers had a surface pore structure and were enriched with a large number of collagen fibers (Fig. 2C). This confirmed the retention of ECM proteins after decellularization and also showed that the cECM microcarriers were conducive to cell adhesion and interactions.

3.2. hADSCs exhibit superior cell behaviors after cECM microcarrier treatment

To determine the regulatory effect of cECM microcarriers on hADSCs and hBMSCs, we first validated the MSC identification criteria developed by the Mesenchymal and Tissue Stem Cell Committee of the International Society for Cellular Therapy (ISCT) in both types of cells [41] (Figs. S1A–C). Next, the cytotoxicity of the microcarriers and their effects on the proliferation and migration of the two types of cells were

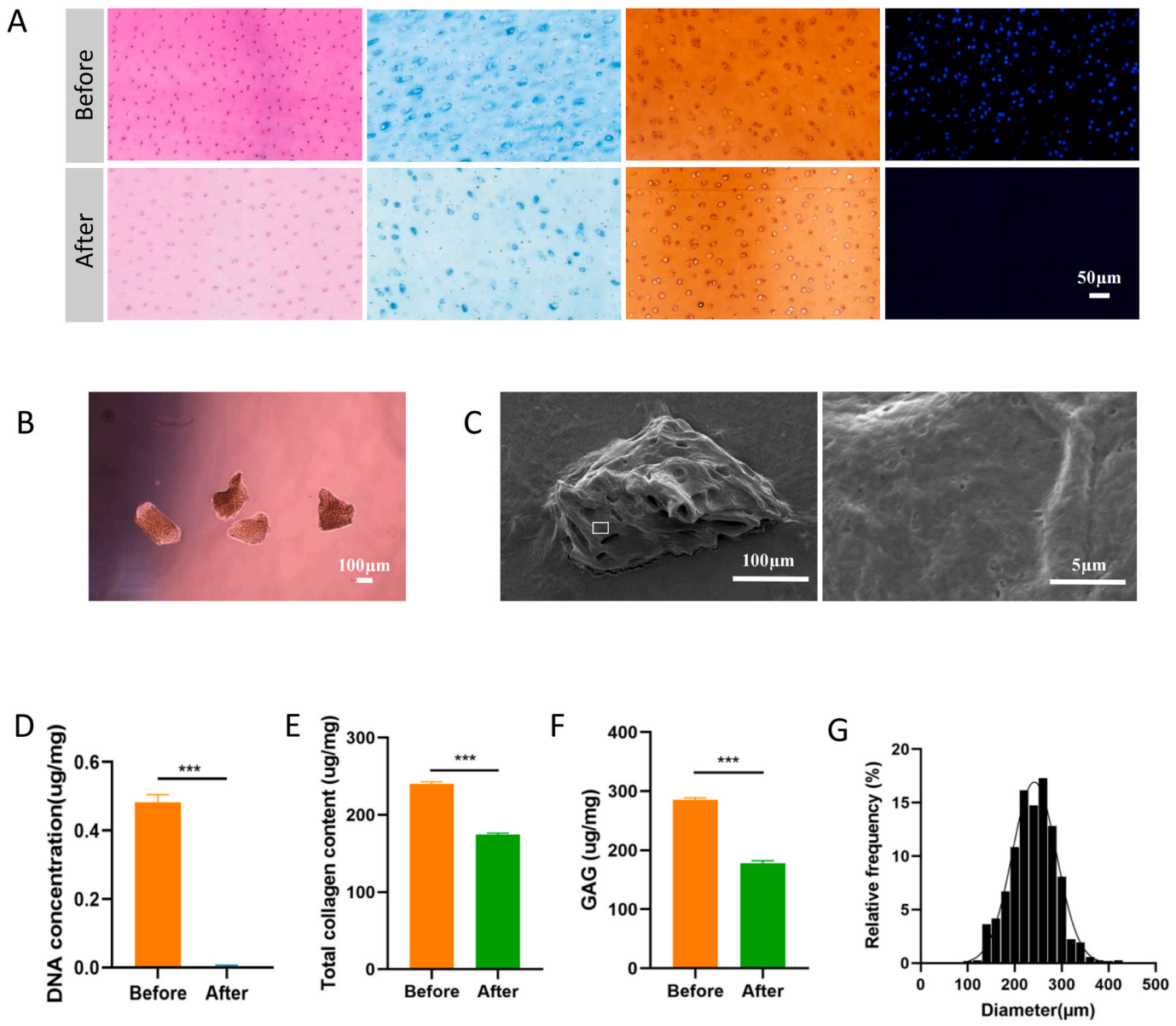

Fig. 2. Characterization of cECM microcarriers. (A) Histological and DAPI staining of cartilage before and after decellularization. (B) Light microscopy images of cECM microcarriers. (C) Scanning electron microscopy images of cECM microcarriers.(D) DNA quantification in cartilage before and after decellularization.(E)Total collagen content of cartilage before and after decellularization. (F)GAG content in cartilage before and after decellularization. (G) The cECM particle size quantification. ***$p < 0.001$.

studied. Both the CCK-8 assay and Ki67 fluorescence staining were used to assess the toxicity of the microcarriers and their effects on cell proliferation. After 1 d, 3 d, and 5 d of treatment, the ADSCs-M and BMSCs-M groups had a higher number of $Ki67^{+}$ cells than the control groups (ADSCs-C and BMSCs-C groups) (Fig. 3A–C). The CCK-8 assay yielded similar results, with the microcarriers promoting the proliferation of both types of cells (Fig. 3B). However, the proliferation of ADSCs was superior to that of BMSCs, irrespective of whether the microcarriers were present (Fig. 3A–C).

Subsequently, we investigated the effects of microcarriers on the migration of the two types of cells using cell migration and Transwell assays. As shown in Fig. 3D, the cells in the ADSCs-M and BMSCs-M groups exhibited faster wound healing than the control cells after 24 h of microcarrier intervention. However, ADSCs showed a more significant healing effect irrespective of microcarrier addition. These findings were further validated through the quantitative analysis of wound area (Fig. 3E). Meanwhile, the Transwell assay was used to assess the effect of microcarriers on vertical migration in both cell types (Fig. 3F). Crystal violet staining after 24 h of microcarrier treatment showed that the number of migrating cells was higher in both the ADSCs-M and BMSCs-M groups than in the control groups, with the number of ADSCs migrating being greater (Fig. 3G). These results indicated that homologous ADSCs were superior to BMSCs in terms of both proliferative and migratory abilities, and that cECM microcarriers could enhance the cellular behaviors of ADSCs.

3.3. *ADSCs-MT has better chondrogenic ability and can recruit more chondrocytes*

The microtissue construction process is shown in Fig. 4A. In order to achieve better microtissue viability, we first performed intermittent slow cell loading (−3 d to −2 d), which was followed by a homogeneous cell proliferation phase (−2 d–0 d), using a dynamic rotary reactor. Then, we induced chondrogenic differentiation via treatment with an

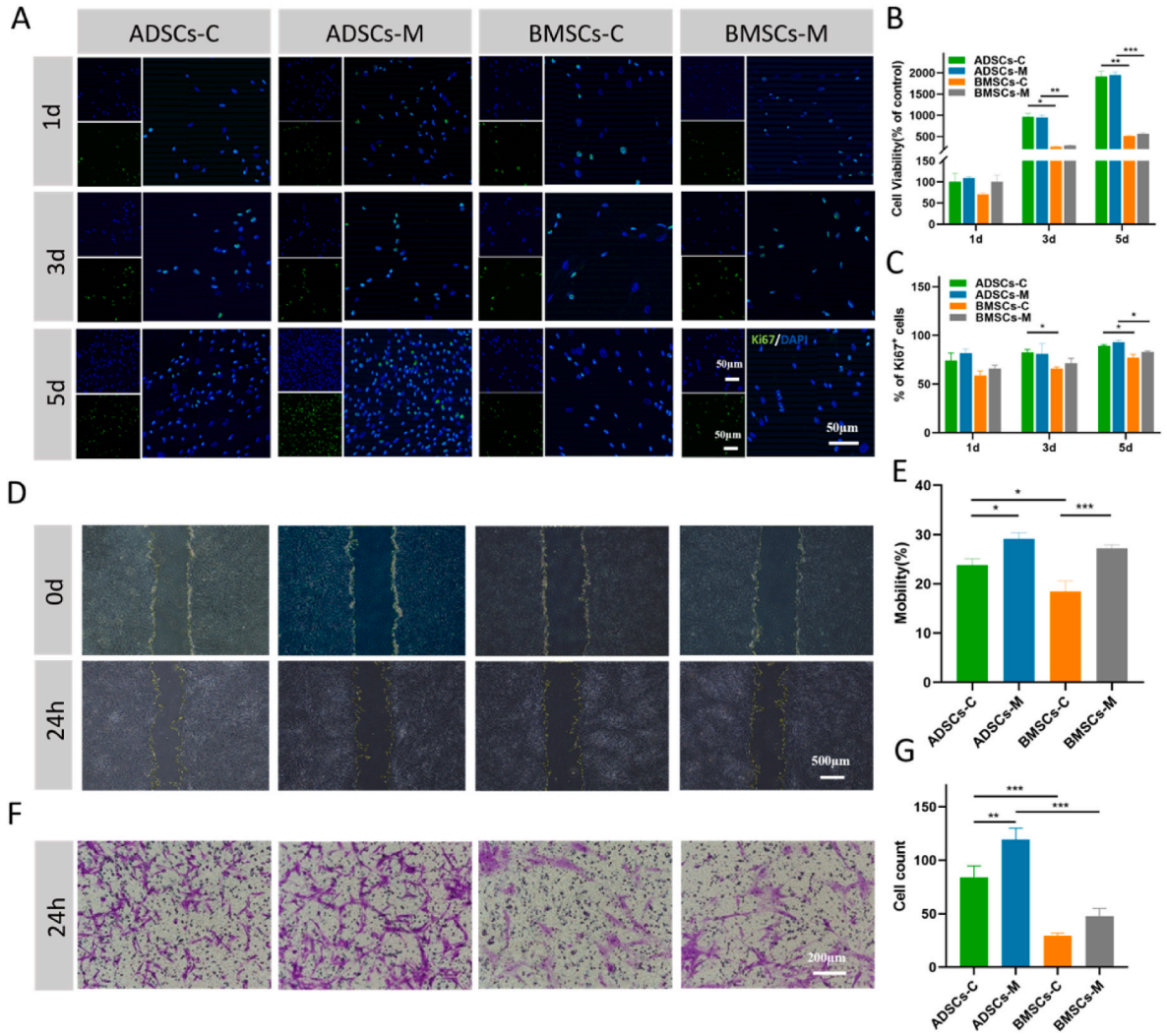

Fig. 3. Effect of cECM microcarriers on the cell behavior of hADSCs and hBMSCs. (A) Immunofluorescence images showing Ki67 staining in the two types of cells treated with cECM microcarriers for different durations. (B) CCK-8 assays for the two types of cells after treatment with cECM microcarriers for different durations. (C) Quantitative analysis of the proportion of $Ki67^{+}$ cells in the ADSCs-M and BMSCs-M groups after treatment with cECM microcarriers for different durations. (D) Cell migration assay. (E) Quantitative analysis of wound healing area. (F) Transwell assay. (G) Quantitative analysis of the number of migratory cells. ADSCs-C: MSCM medium-treated ADSCs (control). ADSCs-M: cECM microcarrier-treated ADSCs. BMSCs-C: MSCM medium-treated BMSCs (control). BMSCs-M: cECM microcarrier-treated BMSCs. $*p < 0.05$, $**p < 0.01$, $***p < 0.001$.

induction medium for 14 d. Throughout the entire fabrication process, a gradual increase in aggregation was observed among the cells in both groups of microtissues (Fig. 4B), with extensive connections gradually being established between the cells and the matrix. Notably, ADSCs-MT exhibited a more compact state of aggregation. Electron microscopy images confirmed the connections of the cells loaded onto microcarriers in both sets of microtissues (Fig. 4C). In ADSCs-MT, the cells showed regular morphology, had a rounded structure, and were more numerous. Meanwhile, in BMSCs-MT, the cells were stretched, showed irregular morphology, and were less numerous. This suggested that the cell proliferation and differentiation properties of cells in ADSCs-MT were superior to those of cells in BMSCs-MT and were more similar to those of mature chondrocytes.

Next, we examined the chondrogenic capacity of the two types of microtissues. We first detected the expression of chondrogenesis-related genes (*SOX9*, COL2, and *ACAN*) and found that all three genes were upregulated in both groups of microtissues after differentiation (14 d) when compared to before differentiation (0 d). Notably, the gene expression levels in ADSCs-MT were higher than those in BMSCs-MT after differentiation (Fig. 4D). In addition, immunofluorescence analysis revealed that SOX9 protein expression was higher in the ADSCs-MT group than in the BMSCs-MT group (Fig. 4E and F), and western blots for ACAN and COL2 further demonstrated the abundant expression of cartilage formation-related proteins in the ADSCs-MT group (Fig. 4G). H&E staining of the two groups of microtissues showed that both cell and ECM densities were higher in the ADSCs-MT group than in the BMSCs-MT group, confirming that both cell proliferation and matrix secretion were superior in the former (Fig. 4H).

Subsequently, we utilized toluidine blue staining to examine the content of glycosaminoglycan components in both groups of microtissues. Compared with the BMSCs-MT group, the ADSCs-MT group exhibited darker staining and a higher content of glycosaminoglycans, consistent with the results of H&E staining. Thus, through chondrogenesis-related gene and protein expression analyses and histological staining, we confirmed the chondrogenic differentiation ability of the two groups of microtissues after dynamic culture. Furthermore, we found that the chondrogenic capacity of ADSCs-MT was superior.

In addition, we used Transwell assays to investigate whether the two types of microtissues could induce the migration of nearby chondrocytes (Fig. 4I), given that the recruitment of endogenous cells in the repair

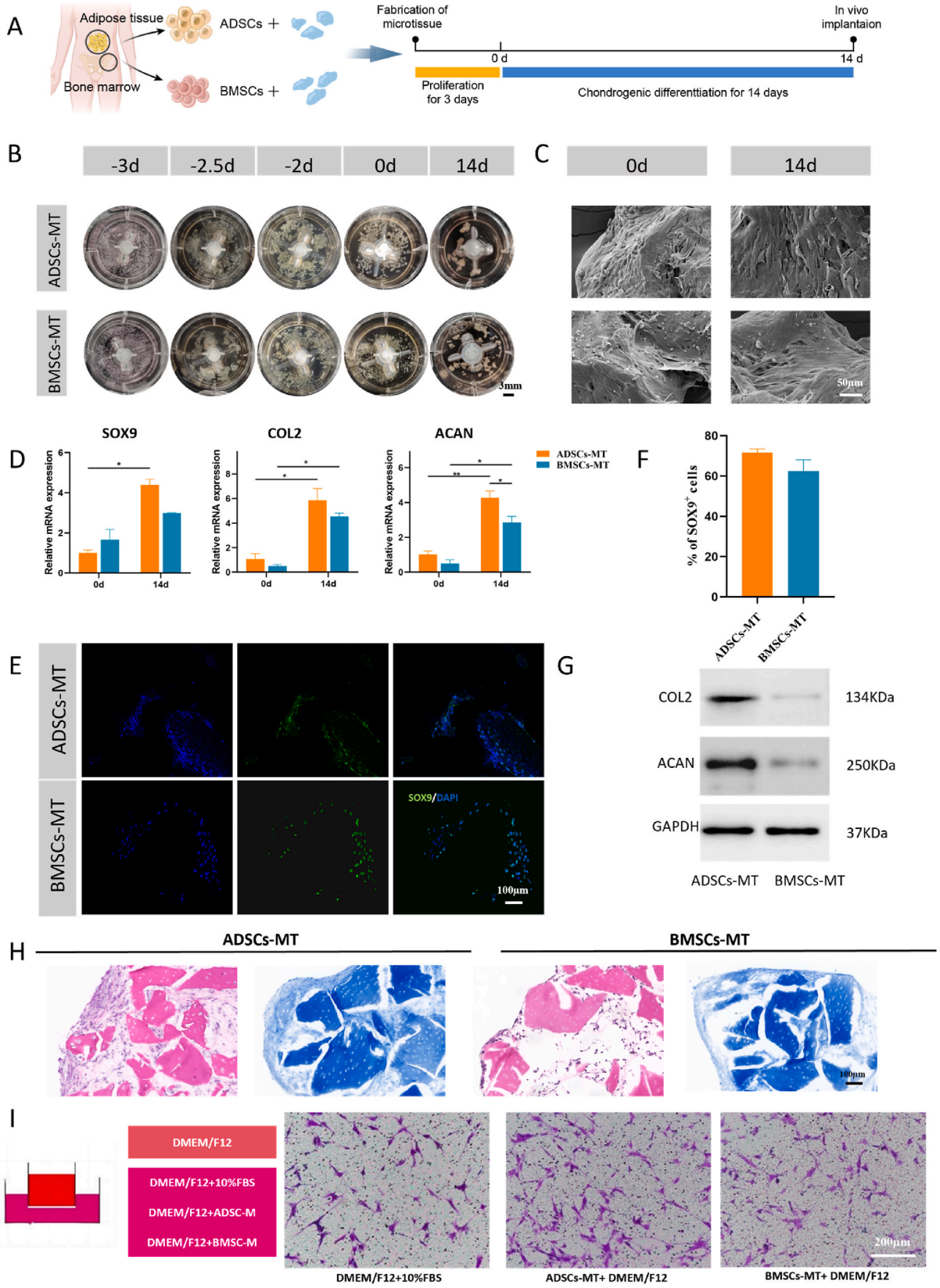

Fig. 4. In vitro evaluation of ADSCs-MT and BMSCs-MT. (A) Schematic diagram showing the microtissue fabrication process. (B) Images representing the key time points in the microtissue fabrication process. (C) Micromorphological observation of the microtissues under SEM (D) mRNA expression of SOX9, COL2, and ACAN in the two groups of microtissues. (E) Immunofluorescence assay for the SOX9 protein in the two groups of microtissues. (F) Quantitative analysis of SOX9 protein expression. (G) Western blot analysis of COL2 and ACAN protein expression in the two groups of microtissues. (H) H&E and toluidine blue staining of the microtissues. (I) Transwell migration assay for three different chemotaxis gradients. $^{*}p < 0.05$, $^{**}p < 0.01$. (For interpretation of the references to color in this figure legend, the reader is referred to the Web version of this article.)

environment enhances repair efficacy [42]. The results showed that ADSCs-MT with BMSCs-MT provided significantly better chemotactic effects than 10 % FBS, and the pro-migration effect of ADSCs-MT on chondrocytes was stronger than that of BMSCs-MT. Overall, compared to BMSCs-MT, ADSCs-MT showed superior chondrogenic and functional effects *in vitro*.

3.4. RNA sequencing analysis of microtissues

To further compare gene expression and regulatory pathways between ADSCs-MT and BMSCs-MT, we subjected the two microtissues to mRNA-seq analysis after differentiation. In total, a total of 9847 genes were expressed in the ADSCs-MT group and BMSCs-MT group (Fig. 5A). Of these, 1039 and 757 genes were solely expressed in ADSCs-MT and BMSCs-MT, respectively. The comparison of DEGs showed that a total of 4034 genes were differentially expressed between the ADSCs-MT group and BMSCs-MT group (2075 up-regulated and 1959 down-regulated) (Fig. 5B). Subsequently, we analyzed the significant DEGs associated with chondrogenic development and degradation and found that the list of genes up-regulated in the ADSCs-MT group (versus the BMSCs-MT group) included acral development -related genes such as *PTN* and *MEF2C* and chondrogenic-related genes such as *SMAD3*, *SMAD4*, *SMAD5*, *COL6A1*, *COL9A1*, and *SOX5*. Meanwhile, the down-regulated differential genes, such as *MMP13*, *ALPL*, *RUNX2*, *BMP2*, *MMP19*, *MMP9*, *IHH*, *COL1A1*, *COL1A2*, and *COL10A1*, were mainly involved in cartilage hypertrophy and matrix degeneration (Fig. 5C).

GO enrichment analysis revealed that the DEGs between the two groups of microtissues were enriched in the pathways — (i) Biological process module: “cell adhesion,” “biological adhesion,” “regulation of signaling,” “Wnt signaling pathway,” and “cell surface receptor signaling pathway”; (ii) Cell components module: “extracellular region,” “myosin complex,” “extracellular region,” and “extracellular matrix”; and (iii) Molecular function module: “growth factor binding,” “signaling receptor binding,” “glycosaminoglycan binding,” and “hyaluronic acid binding”. These pathways were all closely related to the various biological processes of stem cells during chondrogenesis and development (Fig. 5D). In addition, KEGG pathway analysis was conducted, the DEGs were found to be enriched in development-related signaling pathways such as “Hippo signaling pathway” and “signaling pathways regulating pluripotency of stem cells,” as well as stem cell differentiation-related signaling pathways such as “PI3K-Akt signaling pathway,” “ECM-receptor interactions,” “Wnt signaling pathway,” ”TGF-β signaling pathway,” and “glycosaminoglycan biosynthesis-chondroitin sulfate/dermatoxylin sulfate” (Fig. 5E). These results indicated that both groups

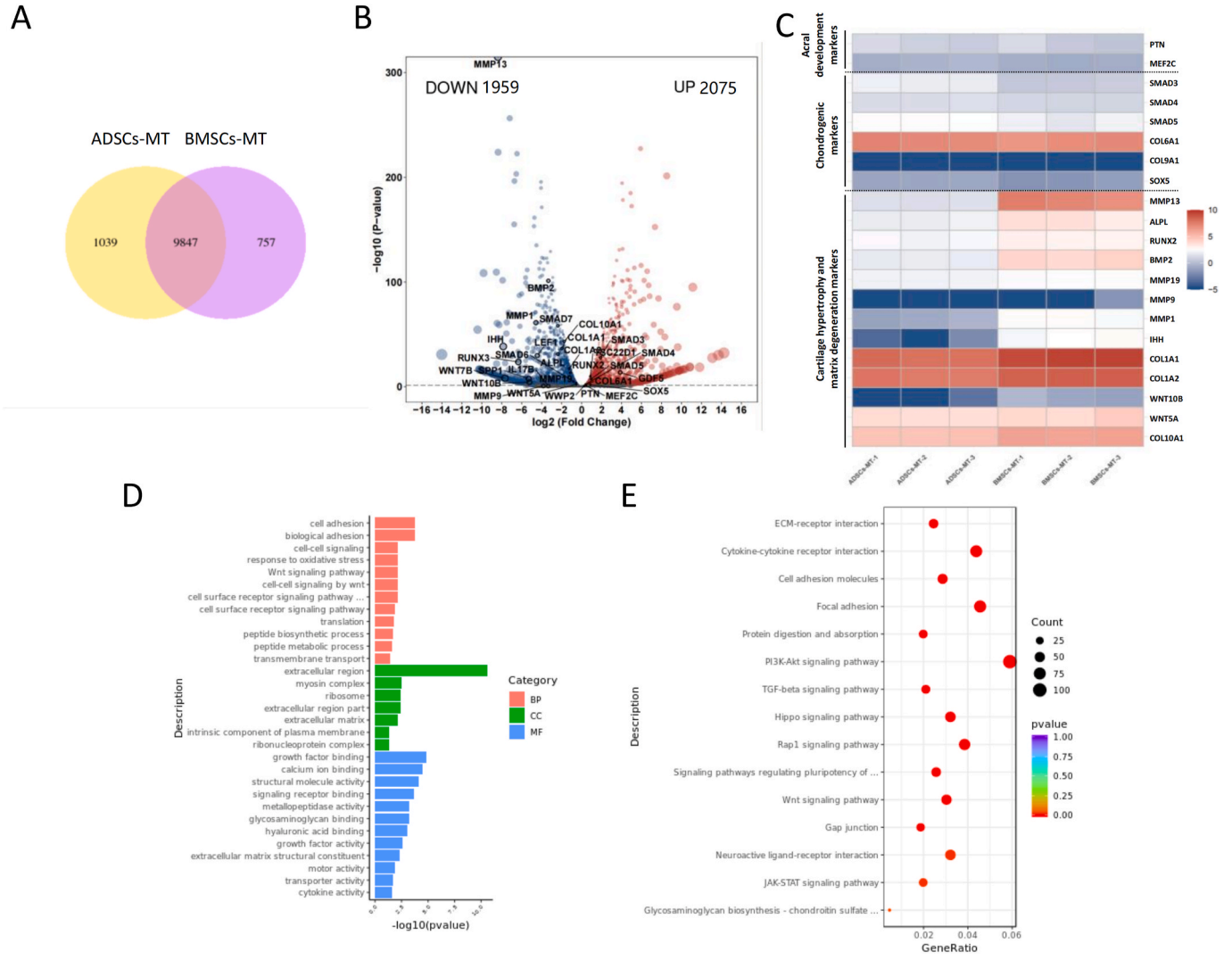

Fig. 5. mRNA-seq and differentially expressed gene (DEG) analysis in the two groups of microtissues. (A) Venn diagram of genes expressed in the two groups of microtissues. (B) Volcano plots of RNA-seq data in the two groups of microtissues. (C) Heatmap of DEGs. (D) GO enrichment analysis of DEGs. (E) KEGG enrichment analysis of DEGs.

of microtissues had a regulatory effect on stem cell development and differentiation. However, ADSCs-MT had a stronger regulatory effect on stem cell development, differentiation, and the inhibition of matrix degradation. These findings also highlighted the potential mechanisms through which ADSCs-MT exerted superior chondrogenic effects compared to BMSCs-MT.

In order to gain insights into the developmental and differentiation processes of ADSCs-MT, we further performed RNA sequencing of ADSCs-MT at key time points during culture (D0, D7, and D14). A total of 9534 genes were expressed in the D0, D7, and D14 groups (Fig. 6A), with 882, 395, and 418 genes expressed exclusively at these time points, respectively. Compared with the D0 group, the D7 group showed 2131 up-regulated and 1551 down-regulated genes. The up-regulated genes were mainly biomarkers related to acral development (e.g., *TNC* and *DLX5*) or early cartilage differentiation (e.g., *SMAD5*, *SMAD4*, and *SOX9*) (Fig. 6B and C). Compared with the D0 group, the D14 group had 2791 up-regulated and 2861 down-regulated genes. Here, the significantly up-regulated genes, such as *COMP*, *SOX5*, *TSC22D1*, and *COL6α1*, were related to cartilage differentiation and matrix composition, while the down-regulated genes, such as *MMP1*, *MMP9*, *IL-1β*, and *VEGFα*, were related to matrix degradation, inflammation, and vascularization (Fig. 6B and D). The process of differentiation between D7 and D14 was also analyzed based on DEGs. Notably, there were 542 up-regulated genes and 604 down-regulated genes in the D14 group versus the D7 group. The findings showed that the differentiation process was characterized by matrix degradation and the down-regulation of vascular biomarkers such as *MMP1*, *MMP13*, *COL10α1*, and *VEGFα* (Fig. 6B and E). Then we validated the relevant key markers through PCR (Fig. 6L–N), confirming that the results demonstrated that the culture of ADSCs-MT mimicked the process of cartilage development and differentiation *in vivo*, followed the transcriptomic gene expression patterns associated with cartilage differentiation, and involved the reduced expression of matrix degradation and vascular markers at the later stage of differentiation. The transcriptomic analysis of DEGs suggested that biomarkers such as *MMP13*, *MMP9*, and *COL10A1* were significantly down-regulated in the ADSCs-MT group versus the BMSCs-MT group, and this significant change mainly occurred from D7 to D14.

Next, we used GO analysis to identify the biological processes associated with the DEGs found between the D0, D7, and D14 groups. We found that these DEGs were involved in regulating various biological processes in stem cells throughout the culture process, including "DNA replication," "regulation of developmental process," "regulation of signal transduction," "extracellular matrix," and "extracellular matrix structural constituent" (Fig. 6F–H). During the early stages of chondrogenesis and differentiation (D7 vs D0), the differential genes were significantly enriched in GO terms related to cell division and development, such as "anatomical structure development," "DNA replication," " chromosome, centromeric region," and "cytoskeletal protein binding," suggesting that the cells remained in a proliferative state in the early stages of culture (Fig. 6F). KEGG pathway analysis at this stage further revealed that the DEGs were significantly enriched in signaling pathways related to cell proliferation ("cell cycle," "DNA replication," and "Rap1 signaling pathway") and signaling pathways for stem cell differentiation ("TGF-β signaling pathway" and "glycosaminoglycan biosynthesis-keratan sulfate") (Fig. 6I). At later stages of culture (D14 vs D7), the differential genes were significantly enriched in GO terms related to chondrogenic differentiation, such as "cell differentiation," "extracellular matrix," and "molecular function regulator" (Fig. 6H). KEGG pathway analysis also showed that at this stage, the DEGs were significantly enriched in pathways related to chondrogenic differentiation, such as "TGF-β signaling pathway" and "Wnt signaling pathway," although signaling pathways related to chondrogenic development, such as "cell adhesion molecules," "calcium signaling pathway," and "Hippo signaling pathway," were also significantly enriched (Fig. 6K). The results demonstrated that the proliferation and differentiation capacities of stem cells were maintained at the transcriptome level in ADSCs-MT throughout the culture period, and the ability to down-regulate matrix degradation and vascular biomarkers was retained. This highlighted the unique advantages of ADSCs-MT in mimicking the *in vivo* complexity of cell fates and chondrogenic differentiation.

3.5. ADSCs-MT exerts stronger paracrine effects and has chondroprotective properties

Through transcriptome analysis, we found that ADSCs-MT can significantly down-regulate genes related to matrix degradation during culture compared to BMSCs-MT. Hence, we asked if this differential expression could in turn affect the properties of surrounding chondrocytes in an inflammatory environment. Typically, MSCs are utilized for cartilage regeneration and repair due to their differentiation ability, while their paracrine effect enhances therapeutic efficacy through cell-to-cell interactions [43]. In order to examine the interaction between the microtissues and human chondrocytes under inflammatory conditions and determine whether the cells in the microtissues retain strong paracrine properties, we utilized a Transwell system and compared the effects of ADSCs-MT and BMSCs-MT on chondrocyte matrix formation- and matrix degradation-related genes and proteins using a co-culture model (Fig. 7A). RT-qPCR (Fig. 7B) showed that, unlike the Blank group, the ADSCs-MT group exhibited a significant matrix-protective effect, as evidenced by the significant increase in the gene expression of *COL2* and *ACAN*, as well as the significant decrease in the gene expression of the matrix-degradation-associated genes *MMP1*, *MMP13*, *ADAMTS4,* and *ADAMTS5*. Similar results were found in the BMSCs-MT group, but the protective effect was not as strong as that in the ADSCs-MT group. The results of protein analysis in the different groups of chondrocytes yielded similar results (Fig. 7C and D), i.e., the protein expression of COL2 and ACAN was the highest in the ADSCs-MT group, followed by the BMSCs-MT group and the Blank group.

MMP13, as a key contributor to articular cartilage destruction, can serve as a marker for the severity of cartilage destruction to a certain extent [44]. Our immunofluorescence assays showed that MMP13 secretion by chondrocytes was significantly reduced in the ADSCs-MT group (Fig. 7E and F). Although MMP13 secretion also showed some degree of reduction in the BMSCs-MT group, the reduction was weaker than that in the ADSCs-MT group. Although the expression of the abovementioned genes and proteins in the ADSCs-MT group could not be restored to normal levels (Control group without IL-1β treatment), a strong inhibition of cartilage degradation and destruction in the inflammatory microenvironment was still observed. This highlighted the chondroprotective effect of ADSCs-MT.

3.6. ADSCs-MT promotes cartilage formation in vivo

We examined tissue regeneration at 8 weeks following the subcutaneous implantation of different microtissues in nude mice based on macroscopic evaluations, histological staining, and immunofluorescence staining. Macroscopic evaluations revealed that the regenerated tissues in the ADSCs-MT group had a cartilage-like appearance, and the tissues were more tightly aggregated. Only a small portion of the GelMA implant was degraded, but it retained its gel-like state. Meanwhile, the regenerated tissue in the BMSCs-MT group was loose in shape, with a cloudy surface and some discrete vascular distribution (Fig. 8A). Histological analysis based on H&E staining revealed that the regenerated tissues in the ADSCs-MT group had high levels of matrix secretion and tight connection. There was no cellular infiltration in the GelMA group, and poor matrix secretion and loose tissue structure were detected in the BMSCs-MT group. This may have affected the subsequent cell-to-cell or cell-to-ECM connections in these groups (Fig. 8B). Both cartilage tissue-specific toluidine blue staining and Safranin O staining showed that the regenerated tissues in the ADSCs-MT group contained abundant ECM, with a more uniform and regular cell morphology and distribution than those in the BMSCs-MT group. The formation of some cartilage lacunas,

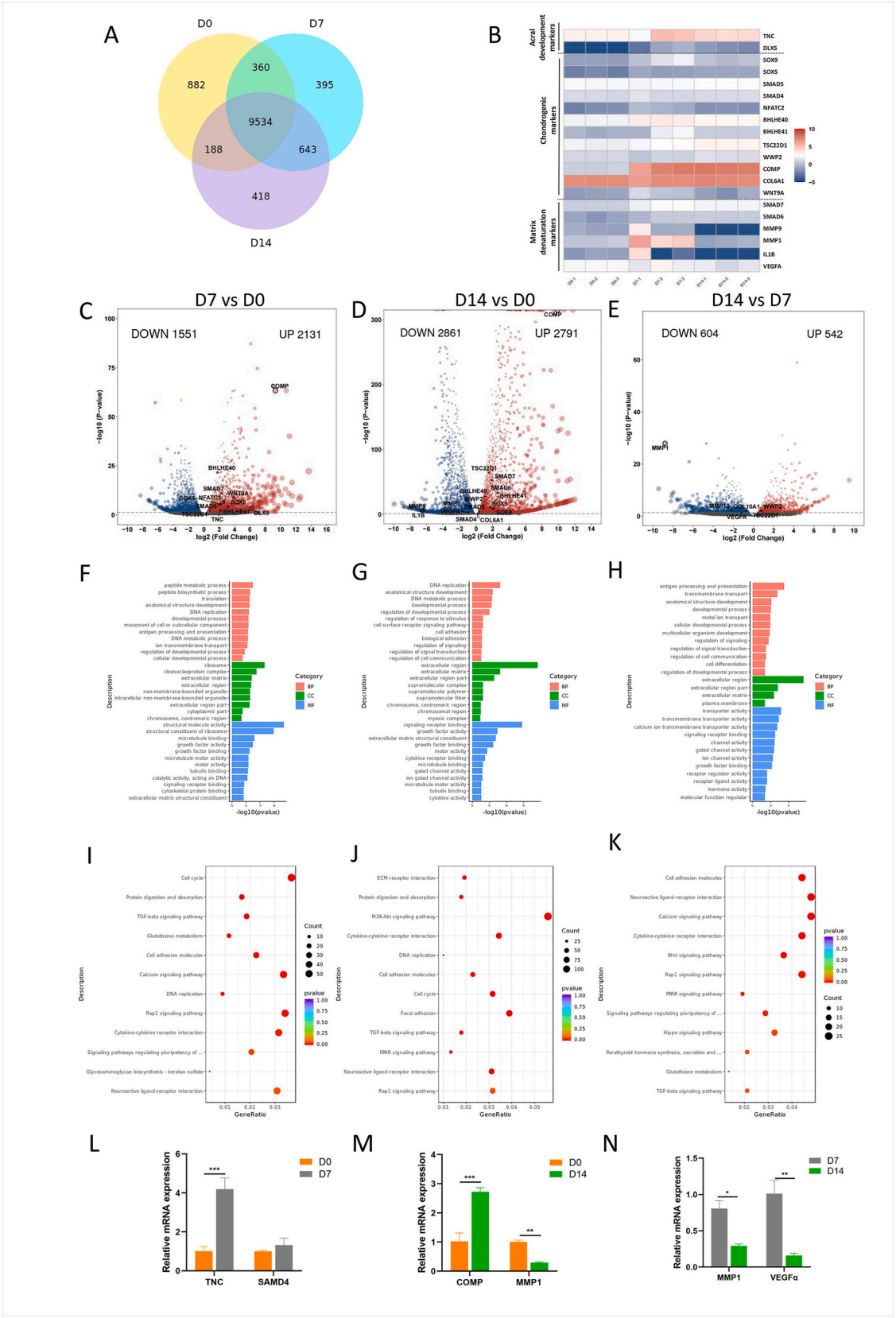

Fig. 6. mRNA-seq and differentially expressed gene (DEG) analysis at key time points during the culture of hADSCs-MT. (A) Venn diagram of genes expressed in ADSCs-MT at D0, D7, and D14. (B) DEG heat map. (C, F, I, L) Volcano plot, GO enrichment analysis, KEGG analysis and PCR validation of DEGs (D7 vs D0). (D, G, J, M) Volcano plot, GO enrichment analysis, KEGG analysis and PCR validation of DEGs (D14 vs D0). (E, H, K, N) Volcano plot, GO enrichment analysis, KEGG analysis and PCR validation of DEGs (D14 vs D7). *$p < 0.05$, **$p < 0.01$, ***$p < 0.001$.

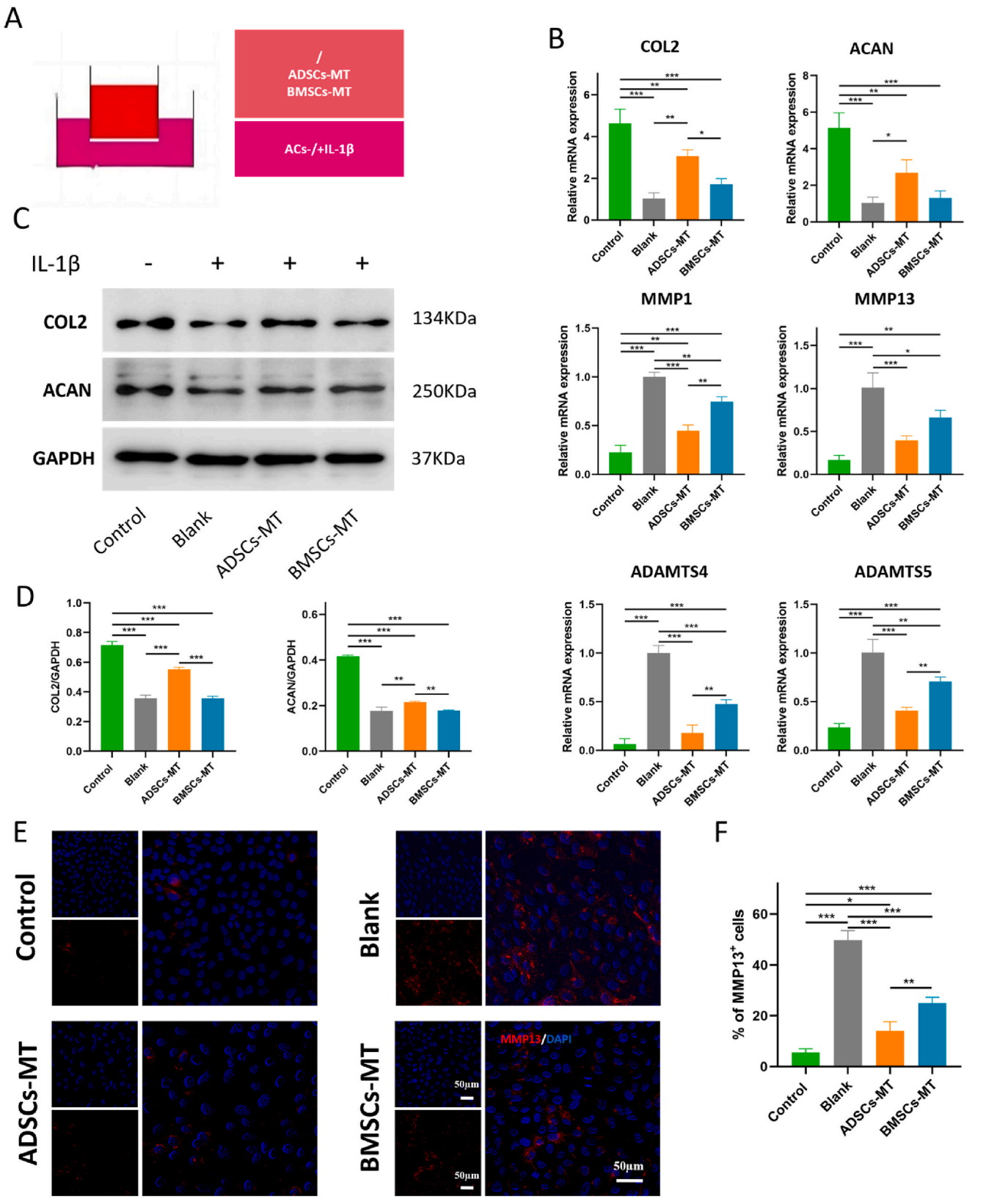

Fig. 7. ADSCs-MT exert chondroprotective effects. (A) Schematic diagram of the Transwell system used to co-culture microtissues with human chondrocytes. (B) Relative expression of matrix formation-related genes (COL2 and ACAN) and matrix degradation-related genes (MMP1, MMP13, ADAMTS4, and ADAMTS5) in the chondrocytes of each group. (C) Protein expression of COL2 and ACAN in the chondrocytes of each group. (D) Quantitative analysis of COL2 and ACAN protein expression. (E) Immunofluorescence analysis of MMP13. (F) Quantitative analysis of MMP13 protein expression based on immunofluorescence assays. $^{*}p < 0.05$, $^{**}p < 0.01$, $^{***}p < 0.001$.

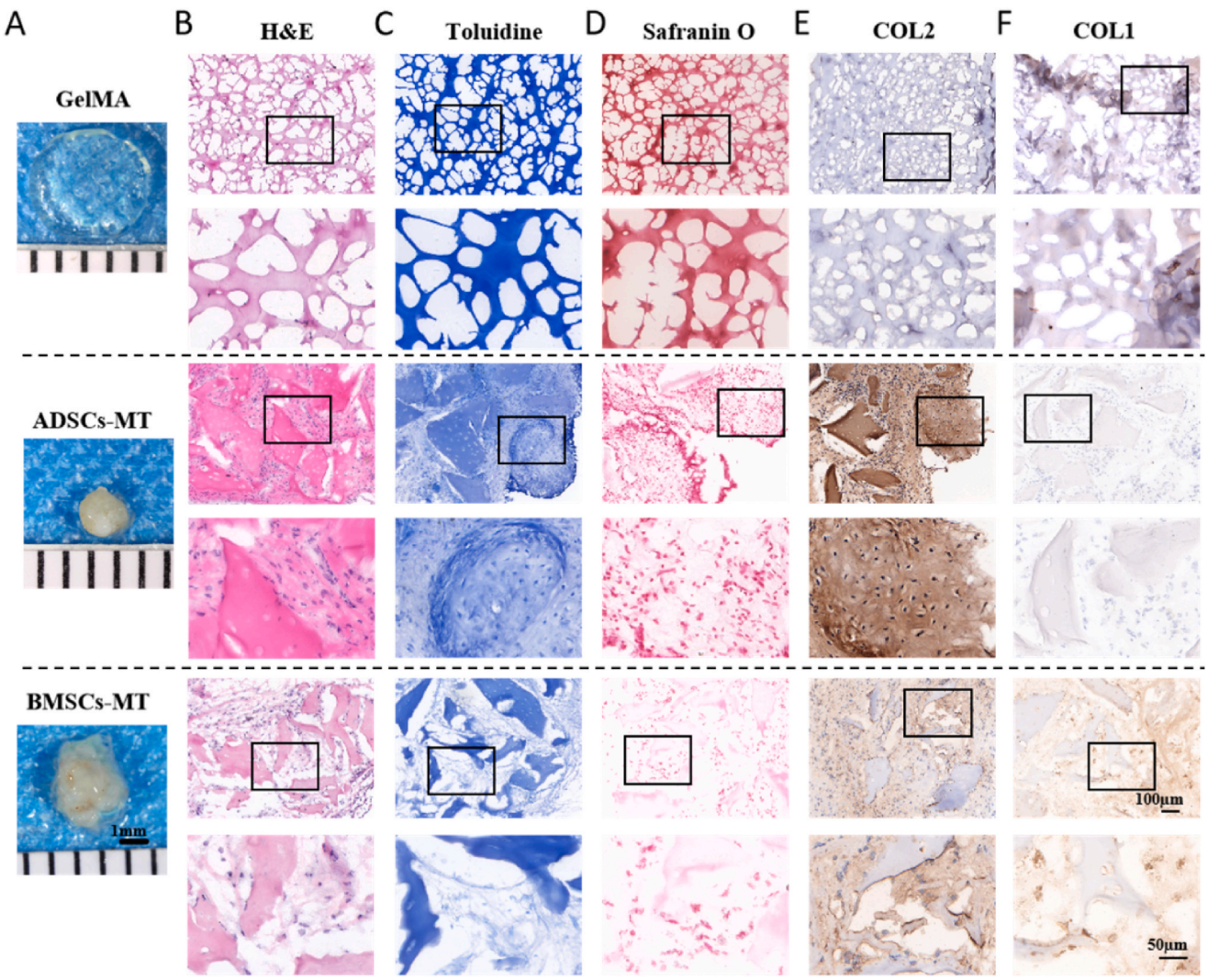

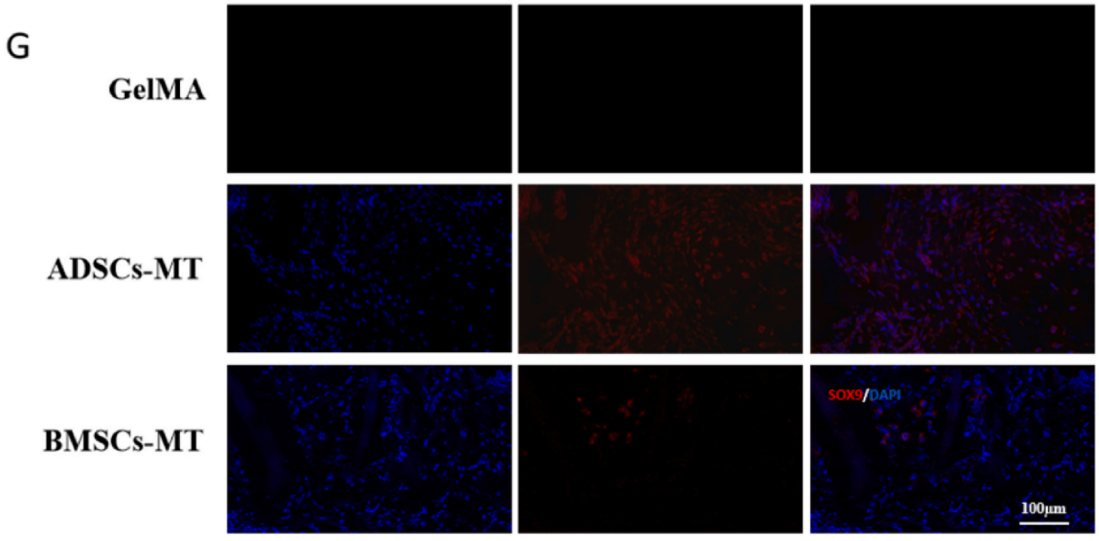

Fig. 8. Evaluation of regenerated tissue in nude mice after 8 weeks of subcutaneous implantation. (A) Gross view of regenerated tissue in each group of nude mice after 8 weeks of subcutaneous implantation. (B) Hematoxylin and eosin staining. (C) Toluidine blue staining. (D) Safranin O staining. (E) Immunohistochemical staining for COL2. (F) Immunohistochemical staining for COL1. (G) Immunofluorescence staining for SOX9. $^{*}p < 0.05$, $^{**}p < 0.01$, $^{***}p < 0.001$. (For interpretation of the references to color in this figure legend, the reader is referred to the Web version of this article.)

a typical feature of chondrocytes in cartilage tissues, was also detected in the ADSCs-MT group [45] (Fig. 8C and D).

In order to better evaluate the matrix composition of the regenerated tissues, we performed immunohistochemical staining for COL2 and COL1. Compared to the BMSCs-MT group, the ADSCs-MT group expressed higher levels of COL2, and an obvious cartilage trap structure and regular cellular morphology could also be observed in this group. Meanwhile, the expression of COL1 was almost absent in the ADSCs-MT group. The absence of cellular infiltration and matrix production was observed in the GelMA group, with low levels of COL1 expression. Meanwhile, the BMSCs-MT group expressed low levels of COL2 and some COL1 (Fig. 8E and F). In addition, immunofluorescence staining for SOX9, a cartilage-specific marker, was clearly stronger in the ADSCs-MT group than in the BMSCs-MT group (Fig. 8G). In summary, the results showed that the ADSCs-MT showed optimal effects in regenerating cartilage tissue, significantly promoting the formation of subcutaneous cartilage in nude mice.

We then utilized a rat knee cartilage defect model for the *in vivo* evaluation of in situ cartilage regeneration. The regeneration of damaged tissue, its integration with surrounding cartilage, and the presence of subchondral bone were assessed through gross visualization and Micro-CT analysis (Fig. S2). The cartilage surface and subchondral bone appeared to show more obvious defects in the Control group, while the cartilage in the GelMA group contained a partially unfilled defect. The cartilage in the ADSCs-MT group had a flatter surface and was better integrated with the surrounding normal tissue, showing a superior repair effect compared to the cartilage in the BMSCs-MT group. The BMD and BV/TV values (Figs. S4B and C) also demonstrated that the tissue health in the ADSCs-MT group was closer to that in the Sham group. ICRS scores (Fig. S4A) were consistent with the macroscopic observations. Finally, H&E staining and Safranin O fast green staining (Fig. S3) was performed to validate the cellular stratification of repaired tissues, evaluate the composition and content of the matrix, and determine histologic scores (Fig. S4D). The superior repair effect in the ADSCs-MT group was validated through the similarity between the layering of repaired tissue and natural cartilage, the deeper coloration on Safranin O staining, the better integration of regenerated tissue with the surrounding tissues, and the flatter repair surface.

4. Discussion

In this study, we constructed two types of microtissues using autologous cells and ECM microcarriers derived from natural cartilage. These microtissues provided a favorable microenvironment for cell adhesion, proliferation, and differentiation. Further, they promoted the regeneration of cartilage matrix to mitigate the threat posed by an inflammatory environment. Microtissues prepared using hADSCs as seed cells were superior to those prepared with hBMSCs as seed cells in terms of cell behavior, chondrogenic capacity, as well as *in vivo* cartilage regeneration.

MSCs possess significant potential for promoting the safe and effective regeneration of articular cartilage due to their robust self-renewal capabilities, high regenerative potential, abundant secretion of bioactive factors (such as chemokines, cytokines, and growth factors), and immunomodulatory properties [46–48]. However, the injection of free MSCs can present challenges, including issues related to cell metabolism, unclear therapeutic effects, and other adverse events [49]. In contrast, microtissue spheres, which are constructed from cells, can replicate the functions of target organs or tissues and have thus been extensively used in disease diagnosis models and therapeutic applications [50,51]. However, microtissues constructed from cell spheres alone have some obvious disadvantages, in that the core cells often fail to survive. Hence, several studies have explored the use of microcarriers to solve such problems [52]. In our study, we employed natural cartilage-derived ECM to prepare microcarriers, which provided an optimal matrix component, as confirmed in our previous studies and the present study. This material created a favorable microenvironment for cell growth and differentiation, enhanced cell-to-cell and cell-to-matrix interactions, and supported the regeneration of cartilage matrix. For example, in proliferation and migration assays, we found that the microcarrier environment significantly promoted cell behavior. Combined with previous findings showing the presence of key cell adhesion-associated proteins, fibronectin, and growth factors within microcarriers [39], such as TGF-β1 may promote cell proliferation through activation of the Smad signaling pathway and enhance migration through remodeling of the ECM and modulation of cell motility [53,54]; insulin-like growth factor 1 (IGF-1) may promote cell proliferation by activating the PI3K/Akt signaling pathway to promote cell survival, proliferation and migration [55].

ADSCs, when used as seed cells, demonstrated a more pronounced effect, with ADSCs-MT showing superior cohesion properties when compared to BMSCs-MT. This was particularly evident after the proliferation phase of ADSCs-MT culture, as demonstrated by imaging analysis as well as the evaluation of micromorphology, gene expression, protein expression, and histology. This highlighted that ADSCs-MT have a more comprehensive effect on matrix regeneration. This may be related to the strong proliferation characteristics of ADSCs. It has been confirmed that the cells adhere to the microcarrier environment suitable for growth and differentiation during the construction of microtissue, and the promoting effect on cell behaviors has been proved. Qi Li et al. found that the high *in vitro* expansion efficiency of ADSCs compared to BMSCs and the strong ability of exosomes to promote chondrogenesis can be attributed to focal adhesion, ECM-receptor interactions, actin backbone regulation, and other factors [56]. We also found in a study by Wenyan Zhou et al. that ADSCs from the same source were more suitable for survival in a hypoxic joint niche than BMSCs and showed advantages in controlling and modulating inflammation and treating osteoarthritis [57]. Furthermore, the 3D dynamic culture provided an enriched nutritional environment for the microtissues, better mimicking the cell behavior within tissues. In previous studies, cartilage microtissues were typically constructed using chondrocytes or stem cells, which generate functional cartilage through their structural and differentiation capabilities [24,25]. In contrast, the present study attempted to leverage the modulation characteristics of the local microenvironment to promote higher-quality chondrogenesis during tissue regeneration, although the sustained *in vivo* effects of the microtissues remain to be confirmed.

In this study, we analyzed the transcriptomes of ADSCs-MT and BMSCs-MT and observed a notable down-regulation of several gene classes in ADSCs-MT. The main down-regulated genes included a series of markers associated with cartilage matrix degradation (e.g., *MMP13*, *MMP19*, *MMP9*, and *MMP1*), those associated with cartilage hypertrophy and early osteogenesis (e.g., *LPL*, *RUNX2*, *BMP2*, and *IHH*), fibrocartilage regulators (e.g., *COL1A2*, and *COL10A1*), and classical inflammatory factors such as IL1-β. These findings pointed to the positive chondrogenic capacity of ADSCs-MT at the RNA level, suggesting a lower likelihood of future ossification and fibrosis when compared to BMSCs-MT. Further transcriptomic analysis of ADSCs-MT at key culture time points was performed to examine the superiority of ADSCs-MT over BMSCs-MT in terms of matrix degradation and down-regulation of fibrocartilage-related markers. This analysis revealed that the changes primarily occurred in the latter half of the culture period.

The vascular environment is known to impact cartilage repair and regeneration. furthermore, the lack of vascularity promotes cartilage formation [58,59]. VEGFα is one of the most critical markers of angiogenesis, and several regeneration studies have shown that high-quality cartilage repair can be achieved by blocking or inhibiting VEGFα expression [45,60]. In the present study, the marker VEGFα was also down-regulated in the second half of ADSCs-MT culture. This down-regulation was in line with the superior cartilage regeneration observed with ADSCs-MT and may have contributed positively toward cartilage homeostasis. GO enrichment and KEGG pathway enrichment analyses further confirmed that, despite these significant changes,

ADSCs-MT retained their inherent features of self-renewal and cartilage formation.

The inflammatory environment has crucial effects on cartilage defect repair and osteoarthritis progression, as it progressively affects the normal chondrocytes in articular cartilage. This leads to pathological changes, such as the secretion of matrix metalloproteinases [44], that hinder cartilage repair. To examine the protective role of microtissues in this context, we employed a Transwell system to co-culture microtissues with chondrocytes instead of performing a direct contact co-culture. This approach was chosen because the microtissues had strong adhesion properties and contained cECM microcarriers. Therefore, direct co-culture analysis would fail to reveal the protective role of the microtissues toward primary chondrocytes. Notably, paracrine function is known to be even more important for tissue-engineered cartilage containing MSCs than the differentiation capacity [47]. Thus, the Transwell co-culture system served as an ideal platform for evaluating the paracrine effects of the microtissues. Following exposure to IL-1β, which promotes inflammation, we assessed the expression of genes and proteins related to chondrocyte matrix formation and matrix degradation in the chondrocytes. We found that the microenvironment of ADSCs-MT was more effective at maintaining the expression of chondrocyte growth factors and matrix markers while inhibiting genes related to matrix degradation, thus exerting a matrix-protective effect. The paracrine function of ADSCs-MT was well-demonstrated and was found to contribute significantly to the therapeutic efficacy of the microtissues. Articular cartilage experiences significant mechanical loading, and its regeneration is dependent on mechanical stimuli [61,62]. It is likely that the mechanical stimuli (i.e., stress and shear) provided by the three-dimensional rotating reactor during microtissue culture modulate the cell behavior and uniform distribution of the ECM. Additionally, these stimuli could influence the secretion of anti-inflammatory and regenerative factors through the modulation of paracrine function, thereby attenuating the destruction of the ECM by the inflammatory environment and regulating the molecular pathways of cartilage regeneration.

Finally, a subcutaneous chondrogenesis model of nude mice and the in situ defect model of rat knee joint cartilage used to assess the *in vivo* regeneration effect of the microtissues, and GelMA hydrogel was used for microtissue encapsulation. The GelMA hydrogel was employed to immobilize the microtissues and enable the delivery of biologically active substances while providing a protective environment where the microtissues could function optimally. The GelMA hydrogel has previously been demonstrated to offer a 3D cross-linked network with good biocompatibility and adequate nutrient supply [45]. However, it was observed that the GelMA hydrogel alone did not support cell invasion or tissue regeneration in the nude mice. Notably, the cartilage tissues regenerated by ADSCs-MT within the GelMA hydrogel exhibited significantly better performance than those regenerated by BMSCs-MT, with obvious differences in the expression of cartilage-related markers such as SOX9 and COL2. While our study did not examine whether the GelMA hydrogel synergistically enhances the effects of ADSCs-MT, the ability of the GelMA hydrogel to improve adhesion and nutrient supply between microtissues and surrounding tissues suggests that it may play a critical integrative and protective role during in situ cartilage repair, thus maximizing the regenerative potential of ADSCs-MT. Combining *in vitro* and *vivo* experiments, we found that the microtissue gradually differentiated into cartilage tissue and secreted abundant cartilage matrix during *in vitro* cultivation. At the transcriptome level, we found that it roughly mimicked the process of cartilage development, formed a cartilage-like tissue *in vitro*, and exerted a protective effect on chondrocytes in the inflammatory microenvironment. After implantation *in vivo*, the cartilage microtissue filled the joint defects, exerted partial cartilage function, and repaired well in the short term.

Although this study verified the excellent chondrogenic ability of ADSCs-MT through systematic evaluations of individual cells, the environmental effects of microcarriers, and various *in vitro* and *in vivo* experiments, it still has several limitations. First, there may have been some variations in the sizes of fabricated microtissues to form clusters, and whether and how potential size differences affect biological functions warrants further exploration. For example, the size and volume of microtissues clusters may affect both specific surface area and cell-cell interactions, which in turn influence cell behavior and function. Microtissues clusters of appropriate sizes may generate a localized hypoxic microenvironment, while moderate hypoxic tension may stimulate cartilage ECM production and promote cartilage differentiation. In the future, we will refine our grouping based on size or volume and explore related differences in oxygen tension, cell behavior, differentiation, and regeneration capacity. Additionally, there is limited research on the mechanical characteristics of microtissues, such as stiffness and elasticity, which are equally important for exploring the mechanism of microtissue action. Finally, we consider increasing the evaluation of the effectiveness of in situ large animal repair in the future, and reducing or controlling the uncertainty and immune rejection of the application of heterologous animal models.

5. Conclusion

This study combined ADSCs and BMSCs with cECM microcarriers, respectively, to construct ADSCs-MT and BMSCs-MT in a three-dimensional dynamic culture environment. A systematic evaluation of the two types of microtissues was conducted through *in vitro* and *in vivo* experiments. The results demonstrated the excellent chondrogenic ability and strong paracrine properties of ADSCs-MT, which can effectively protect inflammatory chondrocytes and promote the regeneration of high-quality cartilage tissue *in vivo*. We believe that this study provides novel insights and evidence for the construction of microtissues and effective enhancement of cartilage regeneration.

CRediT authorship contribution statement

Wei Liu: Writing – original draft, Visualization, Validation, Methodology, Investigation, Formal analysis, Data curation, Conceptualization. **Hongyu Jiang:** Validation, Formal analysis, Data curation, Conceptualization. **Jiajie Chen:** Supervision, Data curation, Conceptualization. **Yue Tian:** Resources, Methodology. **Ying He:** Resources, Methodology, Investigation. **Ying Jiao:** Supervision, Data curation, Conceptualization. **Yanjun Guan:** Software, Resources, Conceptualization. **Zhibo Jia:** Resources, Conceptualization. **Yanbin Wu:** Resources, Data curation, Conceptualization. **Cheng Huang:** Formal analysis. **Yiben Ouyang:** Visualization, Software. **Wenjing Xu:** Resources, Project administration, Funding acquisition. **Jianhong Qi:** Writing – review & editing, Resources. **Jiang Peng:** Writing – review & editing, Project administration, Methodology. **Aiyuan Wang:** Writing – review & editing, Writing – original draft, Project administration, Methodology, Funding acquisition.

Ethics statement

This study obtained written approval from the Institutional Animal Care and Use Committee of Zhongyan Zichuang (Beijing) Biotechnology Co., LTD (No. ZYZC202404019S). The isolation and culture of hADSCs and hBMSCs were approved by the Ethics Committee of the Fourth Medical Centre of the General Hospital of the People's Liberation Army (2020KY036-HS001).

Data and materials availability

All data needed to evaluate the conclusions in the paper are present in the paper and the Supplementary Material.

Declaration of competing interest

The authors declare that they have no known competing financial interests or personal relationships that could have appeared to influence the work reported in this paper.

Acknowledgments

Funding This work was supported by the National Key R&D Program of China (2022YFB3804303),Beijing-Tianjin-Hebei Basic Research Cooperation Program (22JCZXJC00130).

Appendix A. Supplementary data

Supplementary data to this article can be found online at https://doi.org/10.1016/j.mtbio.2024.101372.

Data availability

Data will be made available on request.

References

[1] T.E. Hardingham, A.J. Fosang, Proteoglycans: many forms and many functions, FASEB (Fed. Am. Soc. Exp. Biol.) J. : Official Publication of the Federation of American Societies for Experimental Biology 6 (1992) 861–870.
[2] P. Lu, V.M. Weaver, Z. Werb, The extracellular matrix: a dynamic niche in cancer progression, J. Cell Biol. 196 (2012) 395–406, https://doi.org/10.1083/jcb.201102147.
[3] Z. Peng, H. Sun, V. Bunpetch, Y. Koh, Y. Wen, D. Wu, H. Ouyang, The regulation of cartilage extracellular matrix homeostasis in joint cartilage degeneration and regeneration, Biomaterials 268 (2021) 120555, https://doi.org/10.1016/j.biomaterials.2020.120555.
[4] F. Haghwerdi, M. Khozaei Ravari, L. Taghiyar, M.A. Shamekhi, S. Jahangir, I. Haririan, M. Baghaban Eslaminejad, Application of bone and cartilage extracellular matrices in articular cartilage regeneration, Biomed. Mater. 16 (2021), https://doi.org/10.1088/1748-605X/ac094b.
[5] P. Lepetsos, K.A. Papavassiliou, A.G. Papavassiliou, Redox and NF-κB signaling in osteoarthritis, Free Radic. Biol. Med. 132 (2019) 90–100, https://doi.org/10.1016/j.freeradbiomed.2018.09.025.
[6] W. Zheng, Z. Tao, L. Cai, C. Chen, C. Zhang, Q. Wang, X. Ying, W. Hu, H. Chen, Chrysin attenuates IL-1β-induced expression of inflammatory mediators by suppressing NF-κB in human osteoarthritis chondrocytes, Inflammation 40 (2017) 1143–1154, https://doi.org/10.1007/s10753-017-0558-9.
[7] X.-P. Ge, Y.-H. Gan, C.-G. Zhang, C.-Y. Zhou, K.-T. Ma, J.-H. Meng, X.-C. Ma, Requirement of the NF-κB pathway for induction of Wnt-5A by interleukin-1β in condylar chondrocytes of the temporomandibular joint: functional crosstalk between the Wnt-5A and NF-κB signaling pathways, Osteoarthritis Cartilage 19 (2011) 111–117, https://doi.org/10.1016/j.joca.2010.10.016.
[8] B.S. Kim, H. Kim, G. Gao, J. Jang, D.W. Cho, Decellularized extracellular matrix: a step towards the next generation source for bioink manufacturing, Biofabrication 9 (2017) 034104, https://doi.org/10.1088/1758-5090/aa7e98.
[9] A.H. Morris, D.K. Stamer, T.R. Kyriakides, The host response to naturally-derived extracellular matrix biomaterials, Semin. Immunol. 29 (2017) 72–91, https://doi.org/10.1016/j.smim.2017.01.002.
[10] J.M. Patel, K.S. Saleh, J.A. Burdick, R.L. Mauck, Bioactive factors for cartilage repair and regeneration: improving delivery, retention, and activity, Acta Biomater. 93 (2019) 222–238, https://doi.org/10.1016/j.actbio.2019.01.061.
[11] E.A. Makris, A.H. Gomoll, K.N. Malizos, J.C. Hu, K.A. Athanasiou, Repair and tissue engineering techniques for articular cartilage, Nat. Rev. Rheumatol. 11 (2015) 21–34, https://doi.org/10.1038/nrrheum.2014.157.
[12] H. Kwon, W.E. Brown, C.A. Lee, D. Wang, N. Paschos, J.C. Hu, K.A. Athanasiou, Surgical and tissue engineering strategies for articular cartilage and meniscus repair, Nat. Rev. Rheumatol. 15 (2019) 550–570, https://doi.org/10.1038/s41584-019-0255-1.
[13] S.O. Ebhodaghe, Natural polymeric scaffolds for tissue engineering applications, J. Biomater. Sci. Polym. Ed. 32 (2021) 2144–2194, https://doi.org/10.1080/09205063.2021.1958185.
[14] S. Kim, J.E. Jang, J.H. Lee, G. Khang, Composite scaffold of micronized porcine cartilage/poly(lactic-co-glycolic acid) enhances anti-inflammatory effect, Materials Science & Engineering, C, Materials for Biological Applications 88 (2018) 46–52, https://doi.org/10.1016/j.msec.2018.02.020.
[15] J.E. Barthold, B.M. St Martin, S.L. Sridhar, F. Vernerey, S.E. Schneider, A. Wacquez, V.L. Ferguson, S. Calve, C.P. Neu, Recellularization and integration of dense extracellular matrix by percolation of tissue microparticles, Adv. Funct. Mater. 31 (2021) 2103355, https://doi.org/10.1002/adfm.202103355.
[16] K.H. Hillebrandt, H. Everwien, N. Haep, E. Keshi, J. Pratschke, I.M. Sauer, Strategies based on organ decellularization and recellularization, Transplant International, Official Journal of the European Society for Organ Transplantation 32 (2019) 571–585, https://doi.org/10.1111/tri.13462.
[17] X. Zhang, X. Chen, H. Hong, R. Hu, J. Liu, C. Liu, Decellularized extracellular matrix scaffolds: recent trends and emerging strategies in tissue engineering, Bioact. Mater. 10 (2022) 15–31, https://doi.org/10.1016/j.bioactmat.2021.09.014.
[18] T. Deuse, X. Hu, A. Gravina, D. Wang, G. Tediashvili, C. De, W.O. Thayer, A. Wahl, J.V. Garcia, H. Reichenspurner, M.M. Davis, L.L. Lanier, S. Schrepfer, Hypoimmunogenic derivatives of induced pluripotent stem cells evade immune rejection in fully immunocompetent allogeneic recipients, Nat. Biotechnol. 37 (2019) 252–258, https://doi.org/10.1038/s41587-019-0016-3.
[19] S. Sulaiman, S.R. Chowdhury, M.B. Fauzi, R.A. Rani, N.H.M. Yahaya, Y. Tabata, Y. Hiraoka, R. Binti Haji Idrus, N. Min Hwei, 3D culture of MSCs on a gelatin microsphere in a dynamic culture system enhances chondrogenesis, Int. J. Mol. Sci. 21 (2020), https://doi.org/10.3390/ijms21082688.
[20] S. Tang, P. Chen, H. Zhang, H. Weng, Z. Fang, C. Chen, G. Peng, H. Gao, K. Hu, J. Chen, L. Chen, X. Chen, Comparison of curative effect of human umbilical cord-derived mesenchymal stem cells and their small extracellular vesicles in treating osteoarthritis, IJN 16 (2021) 8185–8202, https://doi.org/10.2147/IJN.S336062.
[21] E.D. Aldrich, X. Cui, C.A. Murphy, K.S. Lim, G.J. Hooper, C.W. McIlwraith, T.B. F. Woodfield, Allogeneic mesenchymal stromal cells for cartilage regeneration: a review of in vitro evaluation, clinical experience, and translational opportunities, Stem Cells Translational Medicine 10 (2021) 1500–1515, https://doi.org/10.1002/sctm.20-0552.
[22] X. Xie, Y. Wang, C. Zhao, S. Guo, S. Liu, W. Jia, R.S. Tuan, C. Zhang, Comparative evaluation of MSCs from bone marrow and adipose tissue seeded in PRP-derived scaffold for cartilage regeneration, Biomaterials 33 (2012) 7008–7018, https://doi.org/10.1016/j.biomaterials.2012.06.058.
[23] L. Zangi, R. Margalit, S. Reich-Zeliger, E. Bachar-Lustig, A. Beilhack, R. Negrin, Y. Reisner, Direct imaging of immune rejection and memory induction by allogeneic mesenchymal stromal cells, Stem Cell. 27 (2009) 2865–2874, https://doi.org/10.1002/stem.217.
[24] Y. Wang, X. Yuan, K. Yu, H. Meng, Y. Zheng, J. Peng, S. Lu, X. Liu, Y. Xie, K. Qiao, Fabrication of nanofibrous microcarriers mimicking extracellular matrix for functional microtissue formation and cartilage regeneration, Biomaterials 171 (2018) 118–132, https://doi.org/10.1016/j.biomaterials.2018.04.033.
[25] MdS. Shajib, K. Futrega, R.A.G. Franco, E. McKenna, B. Guillesser, T.J. Klein, R. W. Crawford, M.R. Doran, Method for manufacture and cryopreservation of cartilage microtissues, J. Tissue Eng. 14 (2023) 20417314231176901, https://doi.org/10.1177/20417314231176901.
[26] J. Colle, P. Blondeel, A. De Bruyne, S. Bochar, L. Tytgat, C. Vercruysse, S. Van Vlierberghe, P. Dubruel, H. Declercq, Bioprinting predifferentiated adipose-derived mesenchymal stem cell spheroids with methacrylated gelatin ink for adipose tissue engineering, J. Mater. Sci. Mater. Med. 31 (2020) 36, https://doi.org/10.1007/s10856-020-06374-w.
[27] J. Zhang, W. Xu, C. Li, F. Meng, Y. Guan, X. Liu, J. Zhao, J. Peng, Y. Wang, Tissue engineering microtissue: construction, optimization, and application, Tissue Eng., Part B 28 (2022) 393–404, https://doi.org/10.1089/ten.teb.2020.0370.
[28] K. Futrega, J.S. Palmer, M. Kinney, W.B. Lott, M.D. Ungrin, P.W. Zandstra, M. R. Doran, The microwell-mesh: a novel device and protocol for the high throughput manufacturing of cartilage microtissues, Biomaterials 62 (2015) 1–12, https://doi.org/10.1016/j.biomaterials.2015.05.013.
[29] K. Futrega, P.G. Robey, T.J. Klein, R.W. Crawford, M.R. Doran, A single day of TGF-β1 exposure activates chondrogenic and hypertrophic differentiation pathways in bone marrow-derived stromal cells, Commun. Biol. 4 (2021) 29, https://doi.org/10.1038/s42003-020-01520-0.
[30] L. Bai, D. Zhou, G. Li, J. Liu, X. Chen, J. Su, Engineering bone/cartilage organoids: strategy, progress, and application, Bone Res 12 (2024) 66, https://doi.org/10.1038/s41413-024-00376-y.
[31] M.T. Cheng, H.W. Yang, T.H. Chen, O.K. Lee, Isolation and characterization of multipotent stem cells from human cruciate ligaments, Cell Prolif. 42 (2009) 448–460, https://doi.org/10.1111/j.1365-2184.2009.00611.x.
[32] J. Kim, Y. Kim, J. Choi, H. Jung, K. Lee, J. Kang, N. Park, Y.A. Rim, Y. Nam, J.H. Ju, Recapitulation of methotrexate hepatotoxicity with induced pluripotent stem cell-derived hepatocytes from patients with rheumatoid arthritis, Stem Cell Res. Ther. 9 (2018) 357, https://doi.org/10.1186/s13287-018-1100-1.
[33] H. Yin, Y. Wang, Z. Sun, X. Sun, Y. Xu, P. Li, H. Meng, X. Yu, B. Xiao, T. Fan, Y. Wang, W. Xu, A. Wang, Q. Guo, J. Peng, S. Lu, Induction of mesenchymal stem cell chondrogenic differentiation and functional cartilage microtissue formation for in vivo cartilage regeneration by cartilage extracellular matrix-derived particles, Acta Biomater. 33 (2016) 96–109, https://doi.org/10.1016/j.actbio.2016.01.024.
[34] S. Hung, H. Cheng, C. Pan, M.J. Tsai, L. Kao, H. Ma, In vitro differentiation of size-sieved stem cells into electrically active neural cells, Stem Cell. 20 (2002) 522–529, https://doi.org/10.1634/stemcells.20-6-522.
[35] J.-P. Wang, Y.-T. Liao, S.-H. Wu, H.-K. Huang, P.-H. Chou, E.-R. Chiang, Adipose derived mesenchymal stem cells from a hypoxic culture reduce cartilage damage, Stem Cell Rev and Rep 17 (2021) 1796–1809, https://doi.org/10.1007/s12015-021-10169-z.
[36] R.I. Dmitrieva, I.R. Minullina, A.A. Bilibina, O.V. Tarasova, S.V. Anisimov, A. Y. Zaritskey, Bone marrow- and subcutaneous adipose tissue-derived mesenchymal stem cells: differences and similarities, Cell Cycle 11 (2012) 377–383, https://doi.org/10.4161/cc.11.2.18858.
[37] H. Yu, Z. You, X. Yan, W. Liu, Z. Nan, D. Xing, C. Huang, Y. Du, TGase-enhanced microtissue assembly in 3D-printed-template-scaffold (3D-MAPS) for large tissue defect reparation, Adv. Healthcare Mater. 9 (2020) e2000531, https://doi.org/10.1002/adhm.202000531.

[38] C. Xie, R. Liang, J. Ye, Z. Peng, H. Sun, Q. Zhu, X. Shen, Y. Hong, H. Wu, W. Sun, X. Yao, J. Li, S. Zhang, X. Zhang, H. Ouyang, High-efficient engineering of osteo-callus organoids for rapid bone regeneration within one month, Biomaterials 288 (2022) 121741, https://doi.org/10.1016/j.biomaterials.2022.121741.
[39] H. Yin, Y. Wang, X. Sun, G. Cui, Z. Sun, P. Chen, Y. Xu, X. Yuan, H. Meng, W. Xu, A. Wang, Q. Guo, S. Lu, J. Peng, Functional tissue-engineered microtissue derived from cartilage extracellular matrix for articular cartilage regeneration, Acta Biomater. 77 (2018) 127–141, https://doi.org/10.1016/j.actbio.2018.07.031.
[40] B. Wang, W. Liu, J.J. Li, S. Chai, D. Xing, H. Yu, Y. Zhang, W. Yan, Z. Xu, B. Zhao, Y. Du, Q. Jiang, A low dose cell therapy system for treating osteoarthritis: in vivo study and in vitro mechanistic investigations, Bioact. Mater. 7 (2022) 478–490, https://doi.org/10.1016/j.bioactmat.2021.05.029.
[41] M. Dominici, K. Le Blanc, I. Mueller, I. Slaper-Cortenbach, F.C. Marini, D.S. Krause, R.J. Deans, A. Keating, D.J. Prockop, E.M. Horwitz, Minimal criteria for defining multipotent mesenchymal stromal cells. The International Society for Cellular Therapy position statement, Cytotherapy 8 (2006) 315–317, https://doi.org/10.1080/14653240600855905.
[42] M. Sani, R. Hosseinie, M. Latifi, M. Shadi, M. Razmkhah, M. Salmannejad, H. Parsaei, T. Talaei-Khozani, Engineered artificial articular cartilage made of decellularized extracellular matrix by mechanical and IGF-1 stimulation, Biomater. Adv. 139 (2022) 213019, https://doi.org/10.1016/j.bioadv.2022.213019.
[43] S. Zhang, S.J. Chuah, R.C. Lai, J.H.P. Hui, S.K. Lim, W.S. Toh, MSC exosomes mediate cartilage repair by enhancing proliferation, attenuating apoptosis and modulating immune reactivity, Biomaterials 156 (2018) 16–27, https://doi.org/10.1016/j.biomaterials.2017.11.028.
[44] Z. Tianyuan, D. Haoyuan, L. Jianwei, H. Songlin, L. Xu, L. Hao, Y. Zhen, D. Haotian, L. Peiqi, S. Xiang, J. Shuangpeng, G. Quanyi, L. Shuyun, A smart MMP13-responsive injectable hydrogel with inflammatory diagnostic logic and multiphase therapeutic ability to orchestrate cartilage regeneration, Adv. Funct. Mater. 33 (2023) 2213019, https://doi.org/10.1002/adfm.202213019.
[45] Y. Chen, W. Chen, Y. Ren, S. Li, M. Liu, J. Xing, Y. Han, Y. Chen, R. Tao, L. Guo, X. Sui, Q. Guo, S. Liu, Y. Han, Lipid nanoparticle-encapsulated VEGFa siRNA facilitates cartilage formation by suppressing angiogenesis, Int. J. Biol. Macromol. 221 (2022) 1313–1324, https://doi.org/10.1016/j.ijbiomac.2022.09.065.
[46] S.M. Richardson, G. Kalamegam, P.N. Pushparaj, C. Matta, A. Memic, A. Khademhosseini, R. Mobasheri, F.L. Poletti, J.A. Hoyland, A. Mobasheri, Mesenchymal stem cells in regenerative medicine: focus on articular cartilage and intervertebral disc regeneration, Methods 99 (2016) 69–80, https://doi.org/10.1016/j.ymeth.2015.09.015.
[47] X. Fu, G. Liu, A. Halim, Y. Ju, Q. Luo, G. Song, Mesenchymal stem cell migration and tissue repair, Cells 8 (2019) 784, https://doi.org/10.3390/cells8080784.
[48] Y.-B. Park, C.-W. Ha, C.-H. Lee, Y.C. Yoon, Y.-G. Park, Cartilage regeneration in osteoarthritic patients by a composite of allogeneic umbilical cord blood-derived mesenchymal stem cells and hyaluronate hydrogel: results from a clinical trial for safety and proof-of-concept with 7 Years of extended follow-up, Stem Cells Translational Medicine 6 (2017) 613–621, https://doi.org/10.5966/sctm.2016-0157.
[49] S. Lopa, A. Colombini, M. Moretti, L. De Girolamo, Injective mesenchymal stem cell-based treatments for knee osteoarthritis: from mechanisms of action to current clinical evidences, Knee Surg. Sports Traumatol. Arthrosc. 27 (2019) 2003–2020, https://doi.org/10.1007/s00167-018-5118-9.
[50] Y. Qiao, Z. Xu, Y. Yu, S. Hou, J. Geng, T. Xiao, Y. Liang, Q. Dong, Y. Mei, B. Wang, H. Qiao, J. Dai, G. Suo, Single cell derived spheres of umbilical cord mesenchymal stem cells enhance cell stemness properties, survival ability and therapeutic potential on liver failure, Biomaterials 227 (2020) 119573, https://doi.org/10.1016/j.biomaterials.2019.119573.
[51] F. Amiri, Co-culture of mesenchymal stem cell spheres with hematopoietic stem cells under hypoxia: a cost- effective method to maintain self-renewal and homing marker expression, Mol. Biol. Rep. (2022 Feb) 931–941. https://orcid.org/0000-0001-8364-7245.
[52] S.-L. Ding, X. Liu, X.-Y. Zhao, K.-T. Wang, W. Xiong, Z.-L. Gao, C.-Y. Sun, M.-X. Jia, C. Li, Q. Gu, M.-Z. Zhang, Microcarriers in application for cartilage tissue engineering: recent progress and challenges, Bioact. Mater. 17 (2022) 81–108, https://doi.org/10.1016/j.bioactmat.2022.01.033.
[53] Y. Ueda, S. Wang, N. Dumont, J.Y. Yi, Y. Koh, C.L. Arteaga, Overexpression of HER2 (erbB2) in human breast epithelial cells unmasks transforming growth factor β-induced cell motility, J. Biol. Chem. 279 (2004) 24505–24513, https://doi.org/10.1074/jbc.M400081200.
[54] Q. Guo, W. Yin, H. Wang, J. Gao, Y. Gu, W. Wang, C. Liu, G. Pan, B. Li, Dynamic proteinaceous hydrogel enables in-situ recruitment of endogenous TGF-β1 and stem cells for cartilage regeneration, Adv. Funct. Mater. (2024) 2403055, https://doi.org/10.1002/adfm.202403055.
[55] A.S. Tarnawski, A. Ahluwalia, The critical role of growth factors in gastric ulcer healing: the cellular and molecular mechanisms and potential clinical implications, Cells 10 (2021) 1964, https://doi.org/10.3390/cells10081964.
[56] Q. Li, H. Yu, M. Sun, P. Yang, X. Hu, Y. Ao, J. Cheng, The tissue origin effect of extracellular vesicles on cartilage and bone regeneration, Acta Biomater. 125 (2021) 253–266, https://doi.org/10.1016/j.actbio.2021.02.039.
[57] W. Zhou, J. Lin, K. Zhao, K. Jin, Q. He, Y. Hu, G. Feng, Y. Cai, C. Xia, H. Liu, W. Shen, X. Hu, H. Ouyang, Single-cell profiles and clinically useful properties of human mesenchymal stem cells of adipose and bone marrow origin, Am. J. Sports Med. 47 (2019) 1722–1733, https://doi.org/10.1177/0363546519848678.
[58] T. Ji, B. Feng, J. Shen, M. Zhang, Y. Hu, A. Jiang, D. Zhu, Y. Chen, W. Ji, Z. Zhang, H. Zhang, F. Li, An avascular niche created by axitinib-loaded PCL/collagen nanofibrous membrane stabilized subcutaneous chondrogenesis of mesenchymal stromal cells, Adv. Sci. 8 (2021) 2100351, https://doi.org/10.1002/advs.202100351.
[59] N. Van Gastel, S. Stegen, G. Eelen, S. Schoors, A. Carlier, V.W. Daniëls, N. Baryawno, D. Przybylski, M. Depypere, P.-J. Stiers, D. Lambrechts, R. Van Looveren, S. Torrekens, A. Sharda, P. Agostinis, D. Lambrechts, F. Maes, J. V. Swinnen, L. Geris, H. Van Oosterwyck, B. Thienpont, P. Carmeliet, D.T. Scadden, G. Carmeliet, Lipid availability determines fate of skeletal progenitor cells via SOX9, Nature 579 (2020) 111–117, https://doi.org/10.1038/s41586-020-2050-1.
[60] A. Marsano, C.M. Medeiros Da Cunha, S. Ghanaati, S. Gueven, M. Centola, R. Tsaryk, M. Barbeck, C. Stuedle, A. Barbero, U. Helmrich, S. Schaeren, J. C. Kirkpatrick, A. Banfi, I. Martin, Spontaneous in vivo chondrogenesis of bone marrow-derived mesenchymal progenitor cells by blocking vascular endothelial growth factor signaling, Stem Cells Translational Medicine 5 (2016) 1730–1738, https://doi.org/10.5966/sctm.2015-0321.
[61] C.S. Chen, Mechanotransduction – a field pulling together? J. Cell Sci. 121 (2008) 3285–3292, https://doi.org/10.1242/jcs.023507.
[62] C. Meinert, K. Schrobback, P.A. Levett, C. Lutton, R.L. Sah, T.J. Klein, Tailoring hydrogel surface properties to modulate cellular response to shear loading, Acta Biomater. 52 (2017) 105–117, https://doi.org/10.1016/j.actbio.2016.10.011.